Identification of Determinants that Allow Maintenance of High-Level Fluoroquinolone Resistance in *Acinetobacter baumannii*

Efrat Hamami[1], Wenwen Huo[1], Arnold Castaneda[3], Jinna Bai[2], Sapna Syal[1], Juan C. Ortiz-Marquez[4,5], Tim van Opijnen[5], Edward Geisinger[1,2] and Ralph R. Isberg[1,*]

[1]Department of Molecular Biology and Microbiology, Tufts University School of Medicine, 150 Harrison Ave., Boston, MA 02111, USA.

[2]Department of Biology, Northeastern University, Boston, MA 02115, USA

[3]Department of Biology, Tufts University, Medford, MA 02155, USA

[4]Department of Biology, Boston College, Chestnut Hill, MA 02135 USA

[5]Innovation Laboratory, Broad Institute, Cambridge, MA 02412, USA

[*]Corresponding Author

Abstract

Acinetobacter baumannii is associated with multidrug resistant (MDR) infections in healthcare settings, with fluoroquinolones such as ciprofloxacin being currently ineffective. Clinical isolates largely harbor mutations in the GyrA and TopoIV fluoroquinolone targets, as well as mutations that increase expression of drug resistance-nodulation-division (RND) efflux pumps. Factors critical for maintaining fitness levels of pump overproducers are uncharacterized despite their prevalence in clinical isolates, so proteins that contribute to fitness of FQR strains overexpressing three known RND systems were identified using high-density insertion mutagenesis. Overproduction of the AdeFGH efflux pump caused hypersensitization to defects in outer membrane homeostatic regulation, including lesions that reduced peptidoglycan recycling and LOS biosynthesis, and interfered with outer membrane lipid asymmetry driven by the Mla system. In contrast, AdeAB pump overproduction, which does not affect the outer membrane pump component, was relatively tolerant to loss of these functions, consistent with outer membrane protein overproduction being the primary disruptive component. Surprisingly, overproduction of proton-transporting efflux pumps had little impact on cytosolic pH, consistent with a compensatory response to pump activity. The most striking transcriptional changes were associated with AdeFGH pump overproduction, resulting in activation of the phenylacetate (PAA) degradation regulon. Disruption of the PAA pathway resulted in cytosolic acidification and defective expression of genes involved in protection from peroxide stress. These results indicate that the RND outer membrane protein overproduction is compensated by cytoplasmic buffering and maintenance of outer membrane integrity in *A. baumannii* to facilitate fitness of FQR isolates.

53

54 **Introduction**

55 *Acinetobacter baumannii* is a Gram-negative bacterium primarily associated with
56 diseases in healthcare settings (1-3). The microorganism has the potential to cause a diverse
57 range of diseases including pneumonia, wound, and urinary tract infections (1-3). Of great
58 concern is its role in causing ventilator-associated pneumonia, which may be closely tied to its
59 ability to grow in biofilms on indwelling devices (2-6). Particularly challenging is the high
60 incidence of multidrug resistant (MDR) *A. baumannii* in hospitalized patients, leaving afflicted
61 individuals with few treatment options (1-3). Although there was a reduction in nosocomial cases
62 in the US from 2013 to 2019, the SARS-CoV2 pandemic saw a large jump in cases that
63 illustrates the difficulties in suppressing diseases by this organism (3). Furthermore, the
64 increasingly common resistance profiles of clinical isolates that are refractory to most
65 antimicrobial therapy regimens indicate that the pathogen poses a continued threat to successful
66 treatment (1-3, 7-10). These clinical isolates include a high proportion that are multi-drug
67 resistant (MDR) or decreased susceptibility to various single agents (1-3, 7-10). This has
68 prompted the World Health Organization to report that *A. baumannii* is a high priority candidate
69 for research and development of new antimicrobials (8). For this reason, there is a high demand
70 for novel antimicrobials or improved combination therapies with which we can combat this
71 pathogen.

72 There are a variety of means by which *A. baumannii* acquires resistance, including the
73 acquisition of drug resistance elements via horizontal gene transfer (HGT), the selection of
74 mutations that inactivate drug target sites, and hyper-expression of preexisting drug egress
75 pumps (11-15). Pathogens not only harbor a multitude of efflux systems, some of which are

76 acquired by HGT, but many have broad substrate specificities (11-15), stimulating efforts to
77 discover effective pump inhibitors (16). Unfortunately, there has been no indication of progress
78 in bringing these inhibitors to the clinic, although several have proven effective in interfering
79 with drug action or synergizing with clinically useful antibiotics using laboratory culture
80 conditions or in animal models (16). Nevertheless, given the relentless patterns of resistance
81 acquisition after the use (and misuse) of single-target antibiotics, a treatment regimen that uses a
82 combination of readily available antimicrobials working in synergy could be effective in
83 interfering with resistance evolution. This study approaches this concept by determining
84 candidate proteins that could be targeted together with clinically-proven classes of antibiotics.

85 One drug class that has reduced effectiveness against nosocomial pathogens is the
86 fluoroquinolones (2, 17). Resistance in clinical isolates, or after growth in the presence of
87 antibiotic under laboratory conditions, primarily selects for mutations that disrupt drug binding
88 to the targets topoisomerases II and IV, encoded for by *gyrA* and *parC* genes respectively (17).
89 In *A. baumannii*, the highest levels of fluoroquinolone resistance (FQR) are found in isolates that
90 have increased expression of drug egress pumps in addition to mutations in the drug targets.
91 These drug egress pumps belong to the resistance-nodulation-division (RND) family, in which
92 overexpression is commonly driven by mutations in regulatory elements that result in
93 constitutive expression (18-23). The three major efflux pumps commonly associated with FQR
94 in *A. baumannii* clinical isolates are encoded for by *adeAB*, *adeFGH*, and *adeIJK*, which are
95 controlled by *adeRS* (encoding a two-component system), *adeL* (a LysR type regulator), and
96 *adeN* (a TetR repressor) regulators respectively (18-23). Among these three, the AdeN-regulated
97 pump is associated with intrinsic resistance to fluoroquinolones, as this is the only RND pump in

98 *A. baumannii* that has measurable levels of expression in the absence of activating mutations (17,
99 22, 23).

100 These pump systems traverse both membranes (24-30), and overproduction requires that
101 the envelope accommodates a large population of protein complexes not present in drug-
102 sensitive isolates, putting potential stress on the inner and outer membrane. Therefore, the
103 stability and assembly of these proteins, as well as the fitness of *A. baumannii* during exponential
104 growth may rely upon bacterial functions that work to maintain cell envelope integrity or prevent
105 intrinsic toxicity of the overexpressed efflux system. Our work focuses on identifying genetic
106 interactions in these high-level FQR strains that allow them to maximize fitness, with the goal of
107 identifying proteins necessary to buffer the deleterious effects of pump hyperexpression that
108 could lead to decreased fitness levels in these strains. Such mutations are predicted to identify
109 targets for drugs that are specifically toxic for pump overproducers.

110 In this study, we used dense transposon sequencing and transcriptomics strategies to
111 identify proteins necessary to maintain fitness of *A. baumannii* efflux pump overproducing
112 strains. We demonstrate that strains harboring overproducing mutations in *adeN* and *adeS* show
113 surprising robustness and identify targets of vulnerability in overproducers of the AdeL-
114 regulated pump. These targets are central players in maintaining cell envelope homeostasis. We
115 also connect the expression of the phenylacetate catabolic pathway as a response to pump
116 overproduction that leads to maintaining cytosolic pH and maximizing protection from reactive
117 oxygen species.

118

119

120 **Results**

121 **Identification of mutations that depress fitness of fluoroquinolone-resistant strains**
122 **overexpressing RND efflux pumps.** To identify genes that are important for maintaining the
123 fitness of strains having high-level fluoroquinolone resistance (FQR), we isolated mutations in
124 the ATCC 17978UN *A. baumannii* strain background that are viable in high concentrations of
125 ciprofloxacin (Materials and Methods). These strains were then subjected to a mutagenesis
126 strategy (Fig. 1A) that identified insertion mutations that had lowered viability in an FQR strain
127 background compared to the wild type (called strain WT) (Fig. 1B). Three FQR strains were
128 interrogated, each of which harbored *gyrA*(S81L) and *parC*(S84L) mutations that are responsible
129 for fluoroquinolone resistance in most Gram-negative organisms and are commonly found in the
130 clinic (called strain GP). The three strains were distinguished from each other by having distinct
131 mutations in loci that regulate the expression of clinically relevant *A. baumannii* resistance-
132 nodulation-division (RND) drug egress pumps. The mutation in the two-component regulatory
133 component *adeS*(R152S) upregulates the AdeAB pump, the activating *adeL*(ΔI335A336)
134 mutation upregulates the AdeFGH pump, while a knockout in the repressor *adeN*(::ISAba1)
135 increases expression of the AdeIJK pump (Fig. 1C). It should be noted under conditions of
136 AdeAB pump overproduction, AdeK is used as the outer membrane component and is expressed
137 at wild type levels in the strain background used in this study.

138 Transposon (Tn) mutagenesis was used to determine candidates important for viability or
139 fitness in either the absence or presence of drug. Between 110,000-150,000 unique transposon
140 mutants were created in all three FQR and the WT strain backgrounds, reaching pool saturation
141 levels of about 37-50% based on targets predicted for the *himar-1* transposon (Materials and
142 Methods). Each bank was sequenced post-harvest and transposon-proximal sequences were

143 amplified to identify the locations of insertions in each strain background and to determine
144 overall pool saturation. This sequence data was also utilized to identify insertion site
145 distributions that were present in each strain, because insertions in genes predicted to be essential
146 or cause fitness defects in a specific pump overproducer strain are predicted to be
147 underrepresented relative to the WT strain. Per our first approach (Fig. 1A), insertion abundance
148 throughout the genome was compared between strain backgrounds using the TRANSIT
149 resampling method to identify genes that have fewer insertions relative to WT in the absence of
150 drug (31) (Fig. 2A, Supp. Table 2), as candidates for genes that are putative conditionally
151 essential targets. These were then displayed by the statistical significance as a function of the
152 insertion abundance in each of the pump overproducer strains relative to WT (Fig. 2A). Among
153 genes identified in this fashion (passing significance criteria adj. $p<0.05$) in the absence of
154 fluoroquinolones were *cyoAB* (*adeL* background), *sodB* (*adeN* background) and *psiE* (*adeS*
155 background) encoding components of the ubiquinol oxidase complex, superoxide dismutase, and
156 a phosphate starvation inducible locus (Fig. 2B). In the case of the ubiquinol oxidase, its function
157 during aerobic respiration as a generator of the proton motive force may play a role in allowing
158 the bacterium to tolerate proton influx resulting from the drug-proton antiport activity of the
159 RND efflux pump (32, 33).

160 To provide support that lowered Cyo activity reduces fitness in the presence of
161 *adeL*ΔI335A336, we used CRISPRi to knock down expression of the *cyoABCDE* operon in the
162 GPL and WT strains and determined growth rates in broth culture. To this end, an
163 anhydrotetracycline (aTc) -inducible dCas9 was inserted at the *att*Tn7 locus in both strains and
164 transformed with a plasmid harboring a constitutive single guide RNA (sgRNA) (Materials and
165 Methods). As a control, the original vector containing a scrambled 20nt sequence (labeled NC-

166 sgRNA) was used. Growth was monitored in cultures grown for 5.5 or 6 hours after dilution to
167 low density in LB and aTc (Supp. Fig. 1A). We saw a fitness defect when expression of the
168 ubiquinol oxidase system was knocked down in both the WT and the GPL strains, with the
169 defect enhanced in the WT treated with 100ng/mL aTc (Supp. Fig. 1A). The extent of effect was
170 difficult to evaluate, in part because the presence of aTc appeared to cause toxicity in the WT
171 strain at this concentration. Quantification of *cyoABCDE* operon transcript levels after aTc
172 addition showed that expression was silenced in both strains at comparable efficiency compared
173 to controls (Supp. Fig. 1B).

174 Notably, there were very few insertions in either the WT or the GPL strain. As a
175 consequence, although the locus was distinguished from others by showing the most highly
176 significant difference in insertion efficiencies (Fig. 2, Supp. Fig. 1C), these differences were
177 measured by degrees of essentiality (Fig. 2B, Supp. Fig. 1C). Therefore, a second strategy was
178 pursued to measure fitness defects during growth in broth culture to attempt to identify more
179 clearcut differences in the two strain backgrounds.

180

181 **The FQR mutants are more vulnerable to disruption of constituents controlling cell**
182 **envelope homeostasis.** To attack this problem using a second approach, multiple small Tn
183 insertion pools (~8-16k unique insertions) were constructed in each background, and each was
184 grown for 7-8 generations in the absence of antibiotic to determine the relative fitness levels of
185 individual gene disruptions (>50,000 unique insertions in total for each background; Materials
186 and Methods). The difference in fitness levels between an individual pump overproducer and the
187 wild type was then determined, and statistical significance was plotted as a function of fitness
188 differences in the two backgrounds (Fig. 3A). In the absence of drug, the GPS mutant was

189 particularly tolerant of insertion mutations relative to the WT control, as only insertions in *lnt,*
190 encoding lipoprotein acyltransferase, showed reduced fitness in the GPS mutant compared to
191 WT (Fig. 3A; Supp. Table 3). In the GPS and GPL strains, loss of function of this gene similarly
192 reduced fitness, but in addition, factors involved in lipid trafficking, LOS synthesis, as well as
193 other functions involved in maintaining outer membrane integrity were identified (Fig. 3A, B).
194 These data indicate that in the absence of antibiotic treatment, the pump overproducers showed
195 differential sensitivity to disruption of pathways that support cell envelope homeostasis.
196 Notably, the GPS strain that shows no upregulation of the outer membrane component of the
197 RND systems was the most tolerant of disruption in these pathways (Fig. 3A,B).

198 To determine if antibiotic treatment increased the spectrum of mutations that sensitize
199 pump overproducers, each of the strains was treated at various ciprofloxacin concentrations to
200 identify conditions that resulted in 20-30% growth rate inhibition (Fig. 3C). Using drug
201 concentrations that reproduced these growth rates, each of the insertion banks was grown 7-8
202 generations in the presence of CIP (Fig. 3C) (17), cultures were harvested, gDNA was isolated,
203 insertion sites were selectively amplified and sequenced, and the abundance of each insertion
204 was determined using the MAGenTA pipeline (17, 34, 35) (Materials and Methods). From these
205 datasets, as in the absence of drug, the differences in fitness levels between an individual pump
206 overproducer and the wild type were used to identify mutants that that preferentially
207 hypersensitize the pump overproducer to ciprofloxacin (Figs. 3D, 3E).

208 In general, treatment with drug increased the number of insertion mutations that resulted
209 in fitness defects in the pump overproducers compared to WT (compare Figs. 3B and 3D).
210 Similar to results in the absence of drug, the primary targets for preferential fitness defects were
211 concentrated in proteins involved in the maintenance of outer membrane integrity, with the GPS

212 strain showing higher tolerance than the GPL strain for mutations in the same pathways (Fig.
213 3D). Furthermore, sensitization of pump overproducers became apparent in the presence of CIP
214 in the presence of a hyperactive BfmRS global regulatory system, which controls envelope
215 homeostasis (36), and disruption of the peptidoglycan interface with the outer membrane (*pbpG*
216 (35)) (Figs. 3D, E). Even so, the magnitude of defects was consistently higher for mutations in
217 the GPL compared to the GPS backgrounds, with mutations in the GPN background often
218 showing intermediate effects (Fig. 3D). These effects correlated well with levels of
219 transcriptional upregulation of the gene for the individual RND outer membrane component in
220 each of the pump overproducer strains and were consistent with the lack of upregulation of the
221 GPS outer membrane component.

222 Knockout mutations of candidates were generated in both the FQR and parent strains via
223 homologous recombination to verify their phenotypes (Materials and Methods). Bacterial growth
224 was then evaluated in the presence of Cip (Figs. 4, 5) at concentrations that yielded comparable
225 growth inhibition across strains (Fig. 3C). Based on this analysis (Fig. 3D, E), knockouts in GPN
226 and GPL (*bfmS* knockouts) and in GPL ($ompA_{Ab}$ knockout) showed increased CIP sensitivity
227 (Fig. 4A). Consistent with the deep sequencing analysis in Fig. 3D, growth defects caused by
228 these deletion mutations were particularly exacerbated in the GPL strain after Cip treatment as
229 compared to the WT strain background (Fig. 4B).

230 To ensure the growth inhibition was a result of pump overexpression, the consequences of
231 crossing the mutations in lower-level resistance GP strain was analyzed in comparison to GP
232 carrying each of the pump overproducers (Supp. Fig. 2A). This allowed a direct comparison to
233 strains that only differ in their levels of pump overproduction. The increase in drug sensitivity
234 when comparing GP carrying the Δ*bfmS* and $\Delta ompA_{Ab}$ to the same lesions in the pump

235 overproducers was again more pronounced in the pump overproducers relative to GP, indicating
236 that pump overproduction requires BfmS and $OmpA_{Ab}$ to effectively tolerate Cip exposure
237 (Supp. Fig. S2). Of particular interest was the behavior of each of the mutants in the GPL
238 background. Both the Δ*bfmS* and Δ*ompA* mutants were highly attenuated for growth in the
239 presence of Cip, with growth plateauing far below that observed for controls (Fig. 4B). For
240 instance, when Δ*bfmS* was crossed into the GPL background, growth plateau was observed at
241 about 10X lower culture densities than that observed for the GPL parent, and 12-20X for the
242 same mutation crossed into WT (Fig 4B). Similarly, when the Δ*ompA* mutation was crossed into
243 GPL, plateaus occurred at 5-8X lower culture density than the GPL parent, and about 8X lower
244 than the same mutation crossed into WT (Fig. 4B; Supp. Fig. S2).

245 Given the strong defects observed with these two mutants, other candidate mutations
246 predicted to interfere with envelope biogenesis were interrogated, including LpsB and PbpG,
247 which showed lowered insertion mutation fitness in the pump hyper-expressors when compared
248 to WT, particularly in the GPL strain (Fig. 5A). Deletion mutations were constructed in WT, GP,
249 GPN and GPL backgrounds, and growth of the eight mutant strains was monitored in the
250 presence of Cip. Loss of PbpG from either the GPN or GPL strain background was particularly
251 detrimental to growth in the presence of low Cip concentrations (Fig. 5). In both GPN and GPL
252 backgrounds, strains having the Δ*pbpG* mutation initiated growth, but culture densities stopped
253 increasing, and there was a dip in densities consistent with disruption of bacterial morphology or
254 lysis (Fig. 5B). It is likely that in the presence of Cip, this mutation selectively hypersensitizes
255 efflux pump overproducers, as the parental GP mutant did not show this phenotype (Supp. Fig.
256 2B). In the case of the Δ*lpsB* mutant, growth plateaued at lower levels when the deletion was
257 analyzed in the GPL mutant (8X lower than parent GPL) as compared to GPN (5-7X lower than

258 GPN), consistent with the *adeL*(ΔI335A336) mutation causing more envelope stress than the
259 *adeN* knockout (Fig. 5B). To ensure that this phenotype was directly due to these null mutations,
260 both deletions were complemented *in trans*. The presence of plasmids harboring these genes
261 restored the fitness of both pump hyperexpressers, with growth in the presence of Cip
262 indistinguishable from the appropriate parents harboring empty vector (Fig. 5C).

263 Both PbpG and LpsB have been described to influence overall levels of
264 lipooligosaccharide (LOS) and full-length LOS of *A. baumannii* (35). We wanted to demonstrate
265 that this was observed in the strain backgrounds described here, so the LOS profiles of these
266 strains were investigated (Fig. 6). Lysates from bacteria grown in broth cultures were separated
267 by SDS-PAGE, LOS was quantified by staining with Pro-Q 300 Emerald and normalized to total
268 protein content (Materials and Methods). No significant differences in LOS was detected
269 between the WT or FQR strain backgrounds in regards to profiles or quantities of products (Fig.
270 6A). The LOS bands were classified as "full" (F) or "intermediate" (I) as representative for their
271 glycosylation levels. The unspecified (U) low molecular mass (LMM) species may be a lipid A
272 precursor such as glycosylated undecaprenyl phosphate lipid carrier/precursor (M.S. Trent,
273 University of Georgia, personal communication).

274 For the various strains harboring the Δ*pbpG* mutant, there were decreased levels of the
275 "U", unspecified LMM species, when compared to WT, with slightly higher yields of the LMM
276 band in the GPL background (Fig. 6B). Furthermore, each showed a very similar migration
277 profile on fractionation when compared to either WT or the various parental strains. In contrast,
278 as expected, Δ*lpsB* mutations resulted in truncated LOS (Fig. 6C). Therefore, LOS is altered by
279 these mutations as previously described that was independent of the strain background tested
280 (35).

281

282 **Maintenance of pH homeostasis in the presence of pump overproduction.** The RND-
283 class egress pumps are known to function as drug-proton antiporters (37). With this in mind, we
284 investigated whether FQR pump hyper-expression causes *A. baumannii* cytosolic pH to become
285 more acidic in the presence or absence of Cip substrate. WT, the high-level FQR strains, and the
286 GP precursor strains were grown to mid-exponential phase and loaded with BCECF-AM dye to
287 determine internal pH (pHi). The pHi values were then determined from a standard curve of cells
288 incubated in pH-adjusted buffers in the presence of CCCP to equilibrate external and internal pH
289 (Materials and Methods). In the absence of antibiotic, the cytosol of GPN, the AdeIJK pump
290 over-expressor, was significantly more basic than the GP parent strain (Fig. 7A), while the
291 cytosolic pH values of the other pump over-producers were otherwise comparable to GP or WT
292 controls (Fig. 7A; one-way ANOVA, multiple comparisons between all strains and GP, $p<0.05$).
293 To determine if the presence of Cip, which should result in proton-Cip antiport, affects internal
294 pH, the experiment was repeated after exposure to Cip at concentrations yielding comparable
295 levels of growth inhibition across strains. Cip treatment lowered the pHi compared to the
296 untreated conditions for all strains. The cytosols of the GPS and GPL strains were fractionally
297 more acidic than the GP strain after CIP addition, but the differences did not rise to the level of
298 statistical significance (Fig. 7B; same tests as in 7A). These data indicate there may be
299 homeostatic mechanisms to neutralize the effects of pump overexpression that act at either
300 transcriptional or post-transcriptional levels. Therefore, the global transcriptional effects of pump
301 overexpression were analyzed in the presence and absence of ciprofloxacin (Fig. 1A, third
302 approach).

303

304 **Large transcriptional changes in response to pump overproduction are limited to the**
305 **AdeL-regulated pump.** To determine if pump overproduction results in transcriptional changes
306 that support fitness, the FQR, low-level resistance GP, and WT strains were cultured in the
307 absence or presence of Cip at concentrations causing 20-30% growth inhibition and analyzed by
308 RNAseq (Materials and Methods). Samples were collected during the exponential phase (A_{600}
309 ~0.5) as well as early post-exponential phase (A_{600} ~1), and differentially regulated genes were
310 identified by comparing the high-level FQR strains and the GP parent strain (Fig. 7C-F; GP vs
311 GPL (C, +Cip) and (D, -Cip), GP vs GPN (E), and GP vs GPS (F), Supp. Table 4). In either the
312 presence or absence of Cip, the GPL strain had the greatest number of differentially expressed
313 genes relative to the control GP strain when compared to the other pump-overexpressing strains
314 (Fig. 7C-F). In fact, hyperexpression of either the AdeS- or AdeN-regulated pumps only altered
315 the gene expression patterns of very few genes, either in the presence or absence of Cip (Fig. 7E,
316 F). This result echoes the Tn-seq analysis of the three overproducer strains, as the *adeL* mutant
317 had the largest set of mutations that lowered fitness relative to WT (Figs. 2, 3, and Supp. Fig. 3).

318 Among the various transcriptional changes resulting from AdeL-regulated pump hyper-
319 expression, the most notable was upregulation of the *paa* operon, which codes for proteins
320 involved in degradation of phenylacetate (Fig. 7C). As confirmation, RNA was isolated from
321 parallel cultures of GP and GPL grown in the absence of drug, and cDNA was prepared for q-
322 rtPCR analysis. Consistent with the RNAseq results, transcript levels of the first gene of the
323 operon, *paaA*, were significantly elevated in the GPL strain compared to the GP parent, with a
324 23-fold increase during exponential phase and a 6-fold increase in post-exponential phase (Fig.
325 8A, B). The other transcriptomic change of note in the GPL strain was the downregulation of the
326 *atpE* gene encoding a component of the F_1F_0 proton translocating ATPase/synthase (Fig. 7D).

327 This parallels other work, which shows that depletion of the ATPase/synthase increases fitness of
328 the GPL strain, consistent with lowered expression acting to allow proper homeostatic regulation
329 of either membrane potential or the intracellular proton environment (unpublished).

330

331 **Depletion of *paaA* alters expression of stress-related genes and lowers intracellular**
332 **pH in the GPL pump hyperexpressor.** The phenylacetate catabolic pathway breaks down the
333 substrate phenylacetate to generate end products that feed into the TCA cycle (38). Previous
334 studies indicate that induction of the *paa* pathway in *A. baumannii* may be a response to stress,
335 as observed after antibiotic treatment (39). Therefore, upregulation of this operon may similarly
336 support the fitness as a response to overproduction of the AdeL-regulated pump. It should be
337 emphasized that *paa* mutants showed no apparent fitness defect in our TnSeq screen that was
338 performed on exponentially-growing bacteria. Consistent with the Tn-seq findings, targeting
339 *paaA* by CRISPRi caused no growth defect in the GPL strain as compared to a parallel non-
340 targeting control strain. Depletion was efficient, as there was a 20-fold knockdown in
341 exponential phase and almost 200-fold in early post-exponential phase compared to the negative
342 control (Fig. 8C, D). This argues that in the absence of phenylacetate degradation that other
343 compensatory pathways may allow fitness to be maintained.

344 The *paa* pathway has been shown to promote resistance to hydrogen peroxide (39, 40), so
345 enhanced expression of the *paa* pathway in the AdeFGH pump hyperexpresser may facilitate a
346 response to oxidative stress and/or other stressors. To test this idea, transcription of a set of
347 oxidative stress genes was probed in the GPL strain by q-rtPCR analysis. Knockdown of *paaA*
348 expression in early post exponential phase yielded reduced transcript levels of *katG, katE*, and
349 *sodC* (encoding two peroxidases and superoxide dismutase, respectively; Fig. 8D). This

350 diminished expression is consistent with previous observations that *paa* null mutants are more
351 sensitive to hydrogen peroxide stress through some previously uncharacterized mechanism (39,
352 40).

353 Internal pH was determined after *paaA* knockdown in the GPL mutant (Fig. 8E, F).
354 Knockdown of *paaA,* the first gene of the large operon, resulted in a significant acidification
355 during exponential growth compared to a nontargeting control (Fig. 8E) (A_{600} ~0.52-0.62). By
356 early post-exponential phase (A_{600}~1.22-1.39), the effect of the knockdown was no longer
357 statistically significant compared to the non-targeting control (Fig. 8F). When the *paa*
358 knockdown cultures were grown to exponential phase and exposed to sub-MIC levels of Cip for
359 45min, the pHi was lower than the non-targeting control, but the difference was not determined
360 to be statistically significant (Fig. 8G; significance determined via unpaired t tests). These data
361 indicate a potential role for this pathway in maintaining pH homeostasis during exponential
362 growth of strains overproducing the AdeL-regulated pump.

363 Given that the *paa* operon has been documented to be associated with a drug stress
364 response, we determined if the expression of the *paa* operon is altered in response to Cip in each
365 of the strains. Based on the RNAseq data in exponential (Fig. 9A) and post-exponential (Fig. 9B)
366 phase, *paaA* transcript levels in all the strains were significantly upregulated in response to Cip
367 exposure as compared to growth in the absence of drug (Fig. 9A, B). These results are consistent
368 with previous results showing that upregulation of the *A. baumannii paa* catabolon occurs in
369 response to drug stress (39). Notably, upregulation of *paa* transcript levels in the absence of drug
370 is a special feature of the GPL strain when compared to the GP parent, and this is not observed in
371 the GPS or GPN strains (Fig. 7D).

372 Previous work has shown that pump hyper-expression and the oxidative stress response
373 are contributors to the development of persistence in the presence of supra-MIC levels of
374 antibiotics (41-44). In particular, the single AdeL mutant promotes persistence in the presence of
375 about 20X MIC levels of Cip (44). We therefore determined if depleting *paaA* expression would
376 interfere with persistence. Depleting *paaA* transcript did not alter the ability of a single *adeL*
377 mutation in the WT background to persist in high levels of Cip when compared to the
378 nontargeting control in AdeL (Fig. 9C). WT with the nontargeting control (WT+NC) was
379 included as a negative control to demonstrate the non-persister phenotype. It is evident that the
380 phenylacetate catabolic pathway responds to stress, modulates the oxidative stress response and
381 pH homeostasis, and documented as maintaining virulence in a number of Gram negative
382 organisms (39, 45-47).

383

384 **Discussion**

385 In this work, we set out to identify proteins that were required to maintain fitness of
386 *Acinetobacter baumannii* strains that overproduce drug efflux pumps. The most surprising result
387 was that *A. baumannii* strains that overproduced the AdeN and AdeS regulated efflux pumps
388 appeared to tolerate overproduction, with few mutations causing specific defects in these strain
389 backgrounds (Fig. 3) and little compensatory transcriptional changes (Fig. 7). In contrast, high
390 fluoroquinolone resistant (FQR) strains overproducing the AdeL-regulated pump showed a range
391 of mutants that lowered fitness relative to the WT control and a more pronounced shift in its
392 transcriptome relative to a *gyrAparC* FQR mutant (GP) as a result of increased pump expression.
393 Whether this is due to overproduction of this AdeFGH pump, which is 1000-fold overexpressed
394 relative to that observed in the GP strain, and/or due to additional downstream effects resulting

395 from the mutation in the regulator AdeL is unclear. An obvious difference between these mutants
396 is that *adeL*-activating mutations results in far higher overproduction of the outer membrane
397 component AdeH than the AdeS- and AdeN-regulated outer membrane components. Most
398 notably, the AdeS-regulated pump was the most tolerant of insertion mutations and had the least
399 transcriptional disruption of the strains studied. With this pump, the outer membrane component
400 AdeK is not overproduced in response to the AdeS activating mutation, so it is predicted to have
401 little effect on outer membrane integrity.

402 We have previously seen the AdeL mutation confers persistence in the face of high levels
403 of Cip (44). We initially encountered mutations in this gene during successive passaging of *A.*
404 *baumannii* in a neutropenic mouse pneumonia model subjected to Cip treatment. Single *adeL*
405 activated mutants were eventually outcompeted by mutations that allow increased Cip resistance
406 as well as increased fitness in the absence of antibiotic (44). Therefore, *adeL* activating
407 mutations impart a fitness cost. We suspect that the lowered growth rate is a consequence of
408 envelope stress (Fig. 3) and could have clinical corollaries. The inability of *adeL* mutants to
409 efficiently compete in immunocompetent animals (44) may mirror drug resistance evolution in
410 hospitals, where immunocompromised patients may act as reservoirs for these variants that
411 eventually act as evolutionary precursors to more fit and higher resistance variants. In this
412 fashion, evolutionary precursors that cause cell envelope disruptions may be compensated by
413 further mutations that allow spread in individuals with intact immune systems.

414 Fitness costs and resistance drivers are important for the evolution of MDR clinical
415 isolates and it is common for a pathogen to employ multiple drug egress systems at a time, which
416 has the potential for accumulated envelope stress (19). Of note, while it appears there is no
417 advantage to overexpressing both AdeIJK and AdeFGH efflux systems simultaneously during

418 Cip challenge (GPNL mutant, Supp. Fig. 5), this was not investigated further in the presence of
419 other drugs nor with the third transporter described in this body of work, AdeAB. This work does
420 emphasize, however, that there is an interplay between fitness costs and fractional differences in
421 drug resistance, and that strains having multiple antibiotic efflux systems may require
422 compensatory mutations to reverse fitness costs.

423 The work described here identified points of vulnerability in the high-level FQR strains,
424 especially the AdeL (GPL) mutant, that may be exploited to re-sensitize MDR strains to this
425 drug. It is evident that GPL heavily relies on determinants that stabilize the cell envelope and the
426 induction of specific stress responses to alleviate stress likely imposed by pump hyper-
427 expression. Furthermore, it may explain why *adeS* and *adeN* pump overproducer mutants appear
428 to be particularly common in clinical isolates, while the presence of *adeL* overproducer mutants,
429 have been difficult to demonstrate.

430 BfmS was one of the candidates identified in our Tn-seq screen. It is one half of the
431 BfmRS two-component regulatory system (TCS), functioning as the histidine kinase sensor
432 which negatively regulates the BfmR response regulator. BfmR in turn controls a large
433 transcriptional network including proteins linked to cell wall biogenesis, capsule production, and
434 outer membrane protein assembly among others (36). It is intriguing that disruption of *bfmS* is
435 detrimental to the fitness of the RND pump hyper-expressors, because disruption had been
436 previously shown to promote *A. baumannii* virulence, drug resistance, and the expression of
437 candidate genes such as *lnt* and *pbpG* (36). Presumably, genes known to be preferentially
438 downregulated when the TCS is activated by loss of BfmS may, in bulk, contribute to the fitness
439 of the FQR strains. Another such protein is OmpA, a major outer membrane protein of *A.*
440 *baumannii* with a periplasmic domain that interacts with peptidoglycan (48, 49), that apparently

441 functions as a low-efficiency non-selective ion channel in a fashion similar to that of *E.coli*
442 OmpA and *Pseudomonas* OprF (50, 51). Transcription of *ompA* is controlled by the BfmRS
443 regulon, indicating that increased sensitivity of a *bfmS* mutant in pump overexpressing strains
444 may be tightly linked to lowering *ompA* gene expression (52, 53).

445 The peptidoglycan recycling factor PbpG, also influenced by BfmS, is a candidate of
446 interest predicting that pump overproduction may cause envelope stress. How proteins that
447 function in cell wall dynamics and LOS biosynthesis interface is still unclear, but both are
448 integral to supporting cell structure and the membrane permeability barrier against external
449 stressors. Peptidoglycan (PG) has been shown to play an important role in supporting the fitness
450 of LOS deficient *A. baumannii* (54). It has been postulated that peptidoglycan (PG)-associated
451 proteins may affect the transport and synthesis of LOS (35). Therefore, mutations in this gene
452 could reduce fitness of pump overproducers either due to direct effects on PG or composition of
453 the outer membrane (OM). Interactions between RND transporters and PG had been previously
454 observed, supporting a direct model for this defect (55, 56). On the other hand, there is also good
455 reason to posit that the effects on LOS or composition of the outer membrane otherwise are the
456 primary reason that the absence of *pbpG* reduces fitness of the overproducers. We have found
457 that loss of the LOS biosynthesis gene *lpsB* causes a fitness defect for pump overproducers that
458 is similar to loss of *pbpG*. Therefore, we hypothesize that the FQR strains are highly susceptible
459 to disruptions in *pbpG* and *lpsB* because of their impact on the composition of the OM and LOS
460 levels. Loss of PbpG may interfere with the proper translocation and assembly of the RND
461 transporter's OMF at the cell surface. The changes in LOS levels and composition could impede
462 the stabilization and intra-pump complex interactions important for their functionality. Also, it
463 has been demonstrated that LPS binds OMPs, and likely mediates the associations between

464 OMPs and the outer membrane, reinforcing membrane integrity (57, 58). Therefore, the pump
465 overproducers may be more susceptible to disruptions in *ompA*$_{Ab}$ because its absence may disturb
466 the permeability barrier as well as hinder the stability of the RND outer membrane component.

467 Other envelope determinants that were identified in our screen have either not shown
468 strong defects or deletion mutants could not be constructed. The most significant was the
469 lipoprotein acyltransferase *lnt* (59). We were unable to acquire a *lnt* deletion mutant in any
470 strain background, indicating total deletions may be lethal, so other strategies are necessary to
471 analyze the locus. The Δ*mlaFEDCB* mutants, however, were constructed and showed weaker
472 phenotypes than anticipated, with only a small defect in the GPL mutant during Cip exposure
473 (Supp. Fig. 4A, B). Other loci, such as candidates like *lpxM* which is integral to the synthesis of
474 hepta-acylated lipid A, which support outer membrane barrier function, have yet to be analyzed
475 (60, 61).

476 If there is a single feature linking together the Tn-seq mutant candidates that have lowered
477 fitness in the presence of efflux pump overproduction, it is that they target proteins associated
478 with cell envelope maintenance. Various studies have demonstrated that cell envelope
479 components can compensate for defects in the membrane to facilitate survival, exemplifying the
480 intricate and interconnected nature of the determinants controlling envelope biogenesis (59, 60).
481 The interplay between the identified targets that control the cell wall and membrane integrity
482 likely controls the functionality of the RND transporters. We postulate that PG, LPS, and other
483 OMPs not identified in this study may serve to support the outer membrane component of the
484 RND pump complexes in the cell membrane while simultaneously supporting membrane barrier
485 integrity. As the cell membrane provides a selective permeability barrier against antimicrobials,
486 any destabilization of this barrier may compromise drug efflux pump function as well as lead to

487 drug influx across a similarly compromised barrier. It should be noted that several of the
488 candidates identified in this work show promise as drug targets that could sensitize RND
489 overproducers to Cip treatment. We saw a 3-fold drop in Cipro MIC in the GPL strain when
490 $OmpA_{Ab}$, LpsB, and PbpG were deleted (Supp. Fig. 4C).

491 Analysis of the transcriptome of the RND overproducers provides further evidence for the
492 induction of cell stress as a consequence of overproduction of the AdeL-regulated pump (Fig. 7).
493 Most notably, the transcription of the phenylacetate operon (*paa*) is induced in response to pump
494 overexpression in the absence of antibiotic treatment. This catabolon has been documented to
495 protect against antimicrobial treatment (39), linking pump overproduction to drug stress. Null
496 mutations in the *A. baumannii*, *Burkholderia cenocepacia,* or *Pseudomonas aeruginosa paa*
497 operons were shown to result in bacterial attenuation in a murine CAUTI or *C. elegans* infection
498 models (39, 45-47). This attenuation may be due to its influence on the expression of virulence
499 associated traits, and/or a putative negative signaling role of the substrate phenylacetate which
500 accumulates in the null mutants (46, 47, 62, 63). *A. baumannii paa* null mutants which exhibited
501 a consequent increase in phenylacetate were shown to attract neutrophils in a zebrafish infection
502 model, promoting clearance (62).We reasoned that the production of substrates from this
503 pathway which feed into the TCA cycle could provide proton relief from proton influx produced
504 by the overproduced pump. Another link between the drug and pump overproduction stress
505 responses is the fact that, although the GPS and GPN overproducer strains do not upregulate the
506 *paa* operon expression in the absence of drug treatment, Cip treatment of these strains does result
507 in activation of *paa* (Fig. 9A, B). This result mimics the effect on *paa* transcription caused by
508 overproduction of the AdeL-regulated pump in the absence of antibiotic. The consequences of
509 loss of *paaA* expression appear mild, as we have no evidence its loss leads to a fitness defect

510 under any condition tested here, and knockdown of this gene had no effect on persister formation
511 by an AdeL-regulated pump overproducer (Fig. 9C). There may be redundant pathways that
512 come into play in the presence of drug pressure or other stress when this pathway is absent that
513 explain our failure to observe a clear phenotype.

514 One clear difference is that the absence of *paaA* led to lowered cytoplasmic pH (Fig. 8E,
515 G). We do not know whether the substrate of *paa*, phenylacetate, is transported out of cells by
516 the RND transporter. If it is not, then it is possible that accumulation of phenylacetic acid may be
517 the basis for the lowered cytosolic pH upon knockdown of the *paa* operon. It may be that this
518 substrate when accumulated can also be a signaling molecule. Indole and paraquat are examples
519 of compounds previously shown to stimulate the expression of genes such as *oxyR* and *soxR* that
520 serve to protect *E. coli* from oxidative stress. The accumulation of these compounds also
521 promotes persistence of the bacterium in the face of antibiotic challenge and contributes to
522 population survival, although coming at a fitness cost (41-43). Additional transcriptomic
523 adaptations in the GPL mutant from loss of *paaA* expression should be explored to better
524 understand the role of the catabolon. Finally, it should be pointed out that loss of the proton-
525 pumping ubiquinol oxidase complex is predicted to cause lowered fitness of the GPL strain,
526 consistent with maintenance of membrane protonmotive force being critical for pump
527 overproduction.

528 Our work indicates that targets involved in supporting the integrity of the *A. baumannii*
529 envelope are associated with maintaining fitness of strains that overproduce efflux pumps. The
530 pump that was most highly overproduced in FQR mutants, the AdeL-regulated pump, was
531 associated with the largest number of genetic requirements for fitness, as well as most disruptive
532 to the host cell transcriptome. The genetic loci identified can be viewed as drug targets for

533 synergy with fluoroquinolones as well, defining pathways that may buffer the stress
534 accompanying increased pump activity. Still unclear is how the phenylacetate degradation
535 pathway is induced in response to the stress identified here, and what physiological role, if any, it
536 plays in supporting the fitness of the strains analyzed in this study. Future work will attempt to
537 expand these studies into analyzing the role of essential proteins in supporting pump
538 overproduction in hopes of identifying potential targets for multidrug therapy targeting drug
539 resistant mutants.

540

541

542 **Materials and Methods**

543 **Bacterial strains and growth conditions**. Bacterial strains used in this work are listed in
544 Table 1. All *Acinetobacter baumannii* strains are derived from ATCC 17978UN. Cultures were
545 grown in lysogeny broth (LB) (10 g/L tryptone, 5 g/L yeast extract, 10 g/L NaCl) or on LB agar
546 plates (LB supplemented with 15g/L agarose) and incubated at 37°C with aeration, as well as
547 shaking or on a roller drum if grown in broth. Unless grown the same day, cultures were
548 typically diluted, incubated to recover after overnight growth, then diluted to A_{600}=0.1-0.001 into
549 either 5-10mL broth or into 96-well plates (Costar), and growth was monitored by measuring
550 A_{600} every hour (broth culture) or every 15min (Epoch 2 or SynergyMx, (Biotek) plate readers.)
551 Superoptimal broth with catabolite repression (SOC) was used for recovery following all
552 electroporations of *E. coli* and *A. baumannii* during cloning or library preparations.
553 Electroporations of *A. baumannii* were performed using 0.1cm gap cuvettes (0.2cm for *E. coli*)
554 and the Gene Pulser (Bio-Rad) at the settings 200 Ω, 25 µF, and 1.8 kV (at 2.2kVd). As needed,

555 LB was supplemented with 10% Sucrose or antibiotics at the following concentrations:
556 ampicillin (Amp): 100ug/mL; carbenicillin (Carb): 50-100ug/mL; gentamicin (Gent): 10ug/mL;
557 chloramphenicol (Cm): 10ug/mL; kanamycin (Kan): 20µg/mL; or ciprofloxacin (Cip): varying
558 concentrations (Sigma).

559

560 **Molecular cloning and mutant construction.** Primers (IDT) and plasmids described in
561 this study as well as their sources are listed in Supplementary Table 1. The AdeS (R152S)
562 mutant was selected for by drug selection in a precursor mutant strain, via plating on
563 LB+Gent10. Single colonies were purified on LB agar plates, and then *adeR* and *adeS* amplified
564 by colony PCR and sequenced (Genewiz) to identify what *adeRS* mutations were acquired. The
565 selected *adeS* mutation (R152S) was introduced into the *gyrA(S81L)parC(S84L)*, or GP
566 (GVA37), *A. baumannii* strain background to create *gyrA(S81L)parC(S84L)adeS(R152S)*, or
567 GPS (EHA105), in a similar fashion as that described before (64). Briefly, the mutant allele was
568 amplified with upstream and downstream flanking sequences to generate a product of about
569 1500bp in length and introduced first into pUC18 by restriction enzyme digestion and T4 DNA
570 ligation. Once propagated in DH5α and sequence confirmed (Genewiz), the mutant allele was
571 introduced into the pJB4648 plasmid by restriction enzyme digestion and T4 DNA ligation and
572 propagated in DH5α λpir. The mutant allele in pJB4648 was then introduced into *A. baumannii*
573 by electroporation and homologous recombination with two selection steps, the first selecting for
574 transformants on LB+Gent10ug/mL agar plates and the second counterselection for $Gent^S$ on
575 LB+Sucrose10% agar plates (during which time these plates were incubated either at room
576 temperature or at 30ºC). The internal, in-frame gene deletion mutants were previously created or
577 constructed during this study via three-way restriction enzyme digestions and ligations (35, 36,

578 64). GPL (EHA23), *gyrA(S81L)parC(S84L)adeL(ΔI335A336),* was similarly constructed. The
579 *adeL(ΔI335A336)* allele was PCR amplified from gDNA isolated from P9 Cy3.2 (44) with
580 flanking regions, cloned into pUC18 then moved into pJB4648 as described before, propagated
581 in XL1 Blues and DH5α λpir *E. coli*, sequence confirmed, then introduced into the GP
582 background by electroporation and homologous recombination. GP was created previously (17)
583 and *gyrA(S81L)parC(S84L)adeN(::ISAba1)* (GVA47), or GPN, generated by plating GP on
584 LB+Cip32ug/mL.

585

586 **LOS analysis.** LOS profiles were examined using Tricine gel electrophoresis of cell
587 lysates as previously described, using lysates from cells grown to mid-log phase, gels stained
588 with Pro-Q Emerald 300 (Invitrogen), and Coomassie Brilliant Blue for total protein staining for
589 sample quantification normalization (35).

590

591 **pHi assay.** Buffers of varying pH were made using 50mL combinations of 0.2M
592 Na_2HPO_4 and 0.2M NaH_2PO_4 (65). 5mM BCECF/AM (Thermofisher) and 0.5mM carbonyl
593 cyanide 3-chlorophenylhydrazone (CCCP; Sigma) were prepared in DMSO and stored at -20oC
594 until use. Methods were adapted from previous literature with modifications (66). Overnight
595 cultures made from individual colonies were diluted the next day for recovery before being
596 diluted again to A_{600} ~0.003 in 8mL LB broth (with or without drug as indicated). In the case of
597 dCas9 strains, single colonies were inoculated into 2mL LB in snap cap tubes and incubated to
598 late exponential phase before diluting into 10mL LB + 100ng/mL anhydrotetracycline (aTc).
599 Cultures were grown to exponential phase (reaching A_{600}=0.4-0.7) after which they were pelleted

600 in 15mL conical tubes at 7500g for 5 min, resuspended in sterile phosphate-buffered saline (PBS,
601 Thermo Scientific), loaded with 20µM BCECF/AM in PBS followed by incubation at 30ºC for
602 30 min in a 96-well v-bottom plate protected from light.

603 Cells in the 96 well plate were diluted 1:4, pelleted at 2000rpm for 5 min, resuspended in
604 LB broth and incubated at 37ºC for 5 min, before pelleting once more and re-suspending in 200-
605 400µl previously prepared mono- and di-basic sodium phosphate buffer at neutral pH
606 (experimental samples) or at a range of pH values (*in situ* standard curve samples). Samples were
607 diluted 1:1 in the neutral or pH adjusted buffers to a final volume of 200µl in a 96-well black
608 plate with a clear, flat bottom (Costar). About 10µM CCCP stock was added to the *in situ*
609 standard curve wells. All samples were mixed via pipetting before fluorescence was read at
610 490ex/535em and 440ex/535em after 5 minutes using a spectrophotometer (Biotek SynergyMx
611 with Gen5 software). Background fluorescence from buffer alone was subtracted from each
612 sample before calculating the ratiometric fluorescence of the calibration curve samples and
613 experimental samples. The experimental sample internal pH was interpolated from the *in-situ*
614 calibration curve using standard curve fitting.

615

616 **Preparation of transposon mutant banks**. Transposon banks with *Himar-1* transposon
617 were created as described (17, 35). 50µl electrocompetent *A. baumannii* cells were
618 electroporated with 300ng pDL1100 (*Himar-1*-Kan^R). Cells were recovered in 1mL SOC broth,
619 placed in 14mL snap cap tubes (Corning) and aerated on the drum roller for 15min at 37ºC. The
620 cells were pelleted and resuspended in 400µl SOC, then spread onto two 150 mm culture dishes
621 containing mixed cellulose ester filters (0.45µm pore size, 137mm diameter; Advantec) that had
622 been placed on top of the SOC agar. Plates were incubated for 1hr at 37ºC before filters were

623 transferred to 150 mm culture dishes containing LB+Kan20µg/mL and incubated overnight
624 (~16hrs) at 37ºC.

625 For mini-Tn10 banks, electrocompetent cells were transformed with 75ng pDL1073
626 (mTn10, Kan^R), with subsequent steps following the same procedure as used for *Himar-1.* CFU
627 counts were determined by grabbing images, determining thresholds and quantifying using
628 Image J. Mutants were pooled from filters by gentle shaking in 50-75mL sterile PBS. Glycerol
629 was added for a final concentration of around 10% and aliquots stored at -80oC until use. About
630 21 independent subpools were created in each strain background (producing around 100,000-
631 150,000 cumulative unique mutants).

632

633 **Cip challenge of transposon banks**. Independent subpools comprising of approximately
634 7,500-16,000 unique transposon mutants were challenged as described (17, 35). Mutant banks
635 were thawed on ice, diluted in 25mL LB broth to an A_{600}=0.1, grown to A_{600}=0.2 at 37ºC, then
636 diluted to A_{600}=0.003 in 10mL LB broth with or without ciprofloxacin of varied concentrations
637 added in parallel cultures. The remaining culture (T_1) was harvested to determine what mutants
638 were present prior to outgrowth and drug challenge. Cultures were incubated for about 8
639 generations (around 170min if untreated, 225min if Cip treated), then harvested (T_2). Drug-
640 treated cultures that exhibited 20-30% growth inhibition were harvested. Cultures were pelleted
641 and stored at -20ºC until all samples were collected. The concentration ranges at which
642 comparable growth inhibition was met for each strain background as well as the average
643 population expansions between T_1 and T_2 with each condition (according to A_{600}) are noted in
644 Supplementary Table 3.

645

646 **Preparation of transposon libraries for sequencing**. As described (17, 35), the gDNA
647 was extracted using the DNeasy Blood and Tissue Kit (Qiagen). Samples were treated with
648 proteinase K during resuspension and incubated at 56ºC with shaking for 1hr before treatment
649 with RNase cocktail (Fisher Scientific) for 8min at 62ºC. The gDNA was quantified with SYBR
650 green then diluted to 7ng/µl in UltraPure water (Fisher Scientific). About 28ng of gDNA of each
651 sample was tagmented using TD buffer and TDE1 enzyme (Illumina) and incubated in a
652 thermocycler at 55ºC for 5min prior to melting at 95ºC for 0.5min. Transposon insertion sites
653 were then amplified using Q5 hot start polymerase (NEB) and 0.6µM Nextera 2A-R and olj638
654 (for *Himar-1* libraries), or olj928 (for Tn10 libraries). The 50µl reactions were incubated at 98ºC
655 for 1min, cycled 30 times through 98ºC for 10sec, 65ºC for 20 sec, and 72ºC for 1min, then
656 finally at 72ºC for 2min. 0.5µl of the first PCR products were used for a second PCR reaction
657 used to introduce indexes with leftward *Himar-1*- or Tn10-specific indexed primers and
658 rightward Nextera indexed primers. The reaction and settings were the same except cycling was
659 shorted to 12 cycles. Amplified products were quantified via 2% agarose tris-acetate-EDTA
660 (TAE) gels using SYBR Safe (Invitrogen) for visualization. The gels were loaded with a known
661 amount of 100bp DNA ladder (NEB) alongside samples of each reaction to quantify their
662 concentrations based on band intensity around 250-600bp using a quantitative gel imaging
663 system. Equal measures of all samples were thereafter pooled and purified via PCR column
664 clean-up (Qiagen). About 17.5 pmol of each pooled sample was reconditioned in an additional
665 50µl reaction with primers P1 and P2. Thermocycler settings were set with a heated lid and
666 incubations at 95ºC for 1min, with slow ramp of 0.1ºC/sec to 64ºC then held for 20sec, and
667 finally 72ºC for 10min. The products were purified once more with the PCR column clean-up kit

668 (Qiagen). Primer olj115 (Tn10) or mar512 (*Himar-1*) was used for sequencing at the Tufts
669 University Core Facility of Genomics with the Illumina HiSeq 2500 (SE50, post pippin size
670 selection for 250-600bp).

671

672 **Sequence analysis and assessment of mutant fitness**. Sequenced reads were processed
673 and analyzed as done previously (17, 34, 35, 67). After demultiplexing, the Nextera adapter
674 sequence was clipped from reads using the fastx_clipper, quality filtered, and reads shorter than
675 20nt were discarded. Reads were mapped to the A. baumannii ATCC 17978 reference genome
676 (https://genomes.atcc.org/genomes/e1d18ea4273549a0) using Bowtie 1.2.2 formatted so only
677 unique and best mapped reads are aligned allowing up to 1 maximum mismatch. Fitness scores
678 were then calculated for each transposon mutant using MAGenTA (67) and scores averaged and
679 aggregated at the gene level across replicates. Insertions in the last 10% of genes were excluded
680 and fitness scores normalized to a set of neutral/pseudo genes. The difference in fitness scoring
681 for each gene disruption was assessed between each FQR strain and the WT drug susceptible
682 strain. Significant fitness differences yielded from the same gene disruption between the
683 different strain backgrounds were identified via multiple t test analysis using the original FDR
684 method of Benjamini and Hochberg with significance falling within the FDR of 5% ($q<0.05$).

685

686 **RNAseq experiment to uncover transcriptional differences between FQR and**
687 **parent strains.** Cultures were grown overnight, diluted to an A_{600} of 0.1 in 10mL LB broth,
688 grown for about 1.5hrs at 37ºC on a drum wheel to approximately mid-log growth, then diluted
689 once more to A_{600} of 0.003 in fresh LB broth with or without ciprofloxacin. Some of these were

690 grown to approximately mid-log phase by incubation for 150-165min (untreated) or for 195-
691 225min (ciprofloxacin treated) as similarly done before (17) and reaching A_{600}~0.445-0.68 and
692 A_{600}~0.39-0.66 respectively. Others were grown to about early stationary for 195-210min
693 (untreated) reaching A_{600}~0.85-1.195 or for 255-270min (ciprofloxacin treated) to A_{600}~0.82-
694 1.125. Of the cultures treated with ciprofloxacin, those that exhibited 20-30% growth inhibition
695 (compared to the untreated culture grown in parallel) were harvested (details provided in
696 Supplementary Table 4). About 1-1.5 A_{600} units of all cultures were harvested and frozen at -
697 80ºC until all samples were collected.

698

699 **Preparing RNA for sequencing.** RNA was isolated from the samples using the RNeasy
700 Mini kit (Qiagen) and prepared for sequencing as described (17, 68, 69) following published
701 protocols (70). Approximately 600ng of RNA was fragmented at 94ºC with 10x FastAP buffer
702 for 2.5min then treated with TURBO DNase, FastAP (Thermo Scientific) (and murine RNase
703 inhibitor; NEB) for 30min at 37ºC. Samples were then purified using Agencourt RNAClean XP
704 (Beckman Coulter) and eluted with 12.5µl of DEPC UltraPure water (Fisher Scientific). 5µl of
705 sample was incubated with 1µl of 100µM barcoded RNA adapters at 72ºC for 2 min before
706 mixed with DMSO (American Bioanalytical), 10x T4 RNA ligase buffer, 100mM ATP, RNase
707 inhibitor murine, T4 RNA ligase, and 50% PEG8000 (NEB) to allow for 3' linker ligation at
708 room temperature for 1.5 hours. The 60 samples were pooled into 5 groups of 12 samples each
709 during purification using RNA Clean & Concentrator (Zymo Research) and all eluted with 16µl
710 DEPC UltraPure water.

711 Ribosomal rRNA was depleted using RNase-H as described (71). Probes complementary
712 to *A. baumannii* ATCC 17978UN 23S, 16S, and 5S rRNA sequences (CP079931.1) were created

713 using 0.design_probe.py and off-target binding predicted using 2.predict_probe_offtarget.py
714 (https://github.com/hym0405/RNaseH_depletion). The 89 devised oligos (IDT) were
715 resuspended into 100µM in UltraPure water, and a master-mix created with 5µl of each probe.
716 For each depletion the RNA was mixed with 1µl of the probe mixture, 0.6µl 1M Tris-HCl pH
717 7.5, 1.5µl 5M NaCl, and DEPC UltraPure water for a final 15µl reaction. They were incubated in
718 a thermocycler with a heated lid at 95ºC for 2min, temperature reduced to 45ºC in 0.1ºC/sec
719 increments and incubated a further 5 min at 45ºC. Meanwhile, RNase-H master mix was
720 prepared for each depletion (3µl Hybridase Thermostable RNase H; Epicentre), 0.5µl 1M Tris-
721 HCl pH=7.5, 0.2µl 5M NaCl, 0.4µl 1M MgCl2, and 0.9µl DEPC UltraPure water) and preheated
722 to 45ºC. Post probe and RNA hybridization, 5µl prewarmed RNase-H mixture was added to each
723 probe-RNA mixture and incubated at 45ºC for 30min. These were then purified twice with 2x
724 SPRI RNAClean XP (Agencourt) and eluted with 13µl DEPC UltraPure water.

725 The RNA preparation was then used as a template for cDNA synthesis. 12µl of sample
726 was incubated with 2µl of 25µM AR2 primer at 72ºC for 2min using 10x AffinityScript RT
727 buffer and enzyme (Agilent Technologies), 0.1M DTT, 100mM dNTPs, and 40U/µl murine
728 RNase inhibitor. After 55min at 55ºC, RNA was then denatured in a 10% reaction volume
729 (adding 2µl to the 20µl cDNA reaction product) of 1N freshly prepared NaOH at 70ºC for 12min
730 before neutralization with 4µl of 0.5M freshly prepared acetic acid. The products were then
731 cleaned with Agencourt RNAClean XP, eluted with 5µl DEPC UltraPure water, incubated with
732 2µl of 40µM 3Tr3 adaptor at 75ºC for 3min with the beads still present, and mixed with 10x T4
733 ligase buffer, DMSO, ATP, PEG8000, and T4 RNA ligase for an overnight 20µl ligation
734 reaction at room temperature. The products were purified with SPRI RNAClean XP (Agencourt)
735 beads twice and finally eluted with 25µl H_20. DNA was amplified from cDNA using 10µl of 5x

736 Q5 reaction buffer and 2.5µl Q5 enzyme (NEB), 0.5µl 100mM dNTPs, 10µl cDNA, 2.5µl
737 primers RTS_Enr_P5 and RTS_Enr_P7_BCXX, and water for 50µl reaction. The reactions were
738 incubated at 98ºC for 3min, cycled at 98ºC for 30 sec, 67ºC for 25sec, and 72ºC for 15sec for 14
739 cycles, and completed at 72ºC for 2min. PCR products were purified once with AxyPrep
740 Magnetic PCR beads (Axygen; Corning). DNA was then quantified by Qubit with the dsDNA
741 HS Assay kit (RNA HS Assay kit was used previously for the quantification of the RNA
742 samples; Thermo Scientific) and about 100nM of each of the 5 subpools was pooled together
743 into 1 sample for sequencing.

744 Throughout sample preparation, 1µl SUPERase-IN RNase inhibitor (Thermo Scientific)
745 was added to samples if they were stored at -80ºC in between steps. RNAse Zap was used
746 continuously on surfaces until cDNA was synthesized. Samples were routinely analyzed by
747 submitting samples for QC fragment analysis at the TUCF Genomics Core. The pooled samples
748 were sequenced at this facility, using a NextSeq550 Single-End High output, with 75 cycles
749 following nanoQC.

750

751 **RNAseq analysis.** Sequences that had been de-multiplexed for the i7 barcodes were then
752 de-multiplexed for the i5 barcodes using fastx_barcode_splitter.pl
753 (https://github.com/agordon/fastx_toolkit/). The 5' anchored adaptor sequences were then
754 trimmed *in silico* using Cutadapt (72). Truseq adaptor sequences were also trimmed *in silico*,
755 disallowing any error, and dropping resulting sequences shorter than 20nt. Sequence data was
756 thereafter analyzed following and modifying published scripts
757 (https://github.com/huoww07/Bioinformatics-for-RNA-Seq). The
758 Acinetobacter_baumannii_ATCC_17978.fasta and Acinetobacter_baumannii_ATCC_17978.gbk

759 files were downloaded from the ATCC genome portal
760 (https://genomes.atcc.org/genomes/e1d18ea4273549a0?tab=overview-tab) to create the STAR
761 genome index (via genomeGenerate with STAR). Annotation GTF files were constructed using
762 Geneious then cufflinks gffread for conversion to strict gtf file. Alignments were then performed
763 using STAR. Subread/1.6.3 was used to get a summary of the sequence data features, then
764 featurecount_stat.R as well as mapping_percentage.R were adapted to analyze and visualize
765 features including mapping efficiency and overview of mapped vs unmapped reads. Using the
766 Tufts cluster on demand R studio app, DESeq2, ggplot2, dplyr, tidyverse, ggrepel, DEGreport,
767 and pheatmap tools were employed to analyze the quality of the data set as well as visualize and
768 deconvolve the contrasting transcriptomic data between the high-level FQR pump overproducing
769 strains and the GP parent strain.

770

771 **qPCR analysis for transcript abundance.** Cultures derived from individual colonies
772 were grown in LB broth to early post-exponential phase. About 1 A_{600} unit of culture was
773 harvested and RNA was extracted using RNeasy (Qiagen). cDNA was synthesized after
774 ezDNase treatment using the SuperScript VILO cDNA kit (Thermo Fisher), then amplified using
775 PowerUp SYBR Green Master Mix (Applied Biosystems) and StepOnePlus Real-Time PCR
776 system (Applied Biosystems) per manufacturer's instructions. The efficiency of target
777 amplification was tested using a standard curve of cDNA at varying dilutions and consequently
778 verified to be greater than 95% for each primer pair used. Three biological replicates were
779 evaluated for each strain and three technical replicates examined per biological sample. To
780 confirm a lack of gDNA contamination, control samples tested in parallel which lacked reverse-
781 transcriptase during cDNA synthesis were included. Transcript levels for each indicated target

782 were compared between each mutant strain and the parental strain (via the comparative $2^{-\Delta\Delta CT}$
783 method) after normalization to that of 16S, the endogenous control. The data is represented in
784 bar plots showing the mean fold difference in transcript levels ($2^{-\Delta\Delta CT}$) ± SEM.

785

786 **MIC determination.** MICs were determined by broth microdilutions. Overnight cultures
787 were diluted to A_{600}=0.1 in 3mL LB broth, incubated to early exponential phase (A_{600}=0.2-0.3),
788 then diluted into a final A_{600}=0.003 in 200ul LB broth in the presence of different dilutions of
789 Cip in a 96-well plate (Costar). Growth was monitored by measuring A_{600} every 15min (Epoch 2
790 or SynergyMx, (Biotek) plate readers). At least three replicates were tested for all 29 strains
791 except for Δ*mlaFEDCB* in the WT strain background (n=2). Cip MIC was determined as the
792 lowest concentration that prevented growth up to 12 hours, where mean A_{600} units did not exceed
793 0.035, and they look like the LB only negative controls. Cip MICs were 256µg/mL (GPS and
794 GPN) and 384µg/mL (GPL).

795

796 **Persistence assay.** The *A. baumannii* strains EHA417 (*adeL*ΔI335A336P_{Tet}*::dCas9*
797 (pWH1266-*paaA*-sgRNA)), EHA418 (*adeL*ΔI335A336P_{Tet}*::dCas9* (pWH1266-NC-sgRNA)),
798 and EHA254 (WTP_{Tet}*::dCas9* (pWH1266-NC-sgRNA)) were incubated in 1.5mL LB in
799 triplicate for 2-3 hours. They were then diluted 1/1000 in 8mL LB + 100ng/mL aTc to induce
800 dCas9 expression and grown to mid-exponential phase. Each culture was then normalized to
801 A_{600}~0.5 with fresh LB containing inducer aTc, then treated with 10ug/mL Ciprofloxacin.
802 Samples of culture (500µl) were removed at timepoints 0, 1, 6, and 24 hours, washed with PBS,

803 then resuspended in PBS and serial dilutions were spotted on LB agar plates for overnight

804 incubation at 37ºC and CFU enumeration the next day.

805

806 # Accession numbers

807

808 # Acknowledgements

809 This work is supported by NIH/NIAID & DOD/DARPA.

810 We thank David Lazinski (Tn plasmids), Germán Vargas-Cuebas (for the GPN mutant), Rebecca
811 Batorsky (bioinformatic help with TRANSIT), Juan Hernandez-Bird (whole genome sequencing
812 of null mutant strains), Yunfei Dai (for communications regarding dCas9 strain generation,
813 sgRNA design, and TRANSIT, and for the pUC-Tn7-GentR-pTet::dCas9 and pWH1266-sgRNA
814 plasmids), Matthew Hall (for help with RNAseq library preparation protocols), and Albert Tai
815 and Irina V. Grinvald at Tufts Genomics Core Facility for communications regarding sequencing
816 and library preparation.

817

818 # Author Contributions

819 R.R.I and E.G. designed the TnSeq study and provided training and support with experimental
820 methodologies. E.H. and R.R.I devised the research. S.S. created mariner banks in the WT strain.
821 A.C. created the mariner banks in the GPN mutant and performed TnSeq experiments with GPN
822 and WT. J.B. performed the LOS experiments and analyses. W.H. provided bioinformatic
823 support during trouble shooting, evaluated the frequency of pump regulator mutants among
824 genomes in the PATRIC database, and ran the DESeq2 bioinformatic workflow for the
825 comparative RNAseq study. E.G. created the vectors used to make two of the deletion mutants

826 and the backbone vector used for gene complementation. E.H. performed the experiments not
827 listed here. E.H. and R.R.I interpreted the results. E.H. and R.R.I wrote the manuscript. E.G
828 reviewed and revised the manuscript.

829

830 **Figure legends**

831 **Figure 1. Uncovering the limitations of high-level FQR strains with enhanced RND pump**
832 **expression.** (A) Diagram for the three experimental approaches as described (Materials and
833 Methods; Biorender). 1) Approach #1: Transposon insertion libraries were created in FQR
834 strains overproducing efflux pumps and the drug susceptible WT strain. Insertion abundance
835 across the genome between the two strain types was compared to identify genes with fewer
836 insertions in the FQR strain background than in WT (see B for example). 2) Approach #2:
837 Transposon insertion banks were challenged with sub-MIC levels of Cip, parallel to those grown
838 without drug. Fitness of all transposon mutants was calculated and compared between the strain
839 types. 3) Approach #3: Strains were grown in presence or absence of Cip to exponential or post-
840 exponential phase in presence or absence of drug and transcriptomic data was obtained to
841 discover differentially regulated pathways. (B) Example of insertion abundance in a single gene
842 cluster in two strain backgrounds. (C) Activating mutations in efflux pump regulatory mutants
843 specifically activate their cognate pumps. RNA was isolated from the noted strains and relative
844 transcription determined by q-rtPCR (Materials and Methods). Displayed is mean fold change ±
845 SEM of each target as compared to the parental GP strain. At least three independent biological
846 replicates were used for each strain. FQR: fluoroquinolone resistant. Mid: mid exponential
847 phase. EPE: early post-exponential phase. Cip: Ciprofloxacin. Untx: untreated. WT: wildtype.
848 GPL: *gyrAparCadeL*. GPN: *gyrAparCadeN*. GPS: *gyrAparCadeS*. GP: *gyrAparC*.

849

850 **Figure 2: Discovery of genes with lowered tolerance for insertions in the high-level FQR**
851 **strains.** (A) Volcano plots in which statistical significance is plotted as a function of the
852 differences in insertion abundance between each FQR strain and WT based on TRANSIT
853 algorithm (31). All adjusted p-values = 0 were assigned the value of 0.005 to allow graphing.
854 Blue: genes with adjusted p-values<0.05. Values for all other genes are shown in grey. (B)
855 Number of reads plotted as a function of insertion site for noted genes as well as flanking
856 regions. Shown are: FQR: fluoroquinolone resistant. WT: wildtype. GPL: *gyrAparCadeL*. GPN:
857 *gyrAparCadeN*. GPS: *gyrAparCadeS*.

858

859 **Figure 3: Maintenance of cell envelope homeostasis supports the fitness of efflux pump**
860 **overproducer strains.** (A, E): Statistical significance plotted as a function of relative fitness
861 comparing identical mutations in FQR and WT strains grown in the absence (A) or presence (E)
862 of sub-MIC levels of Cip. (C) Growth rates at noted Cip concentrations to identify conditions
863 allowing 20-30% growth inhibition in the FQR and WT strains. (A) Blue or (E) Red (B):
864 Mutations above the FDR = 5%, q<0.05 as determined by Benjamini and Hochberg (73).
865 Notable findings are labeled. All q-values < 0.000001 assigned the value of 0.000001 for
866 graphing purposes. (B, D) Heatmaps showing fitness of insertions in each gene in noted strain
867 backgrounds. Selected genes with Tn-disruptions yielding lowered fitness in the FQR strains are
868 shown, in the absence of drug treatment (B) or in the presence of Cip (D). Gene names are
869 followed by accession numbers which are preceded by "NDEONHPJ_" per the ATCC 17978
870 strain annotations. Shown are: WT: wildtype. GP: *gyrAparC.* GPS: *gyrAparCadeS.* GPN:
871 *gyrAparCadeN*. GPL: *gyrAparCadeL*.

872

873 **Figure 4: OmpA and BfmS are critical fitness determinants for *adeL*ΔI335A336 strains**
874 **during Cip exposure.** (A) The Single Fitness pipeline of MAGenTA was used to evaluate the
875 fitness of Tn mutants at each position across the loci shown all post Cip treatment. (B) Null
876 mutants in the FQR strain backgrounds grown in the presence of Cip compared to the WT
877 background. Growth was monitored by taking absorbance measurements every 15 minutes in 96
878 well plates in presence of Cip. Displayed are means ± SEM (n≥3). Ciptx: Ciprofloxacin treated.
879 WT: wildtype. GPL: *gyrAparCadeL*. GPN: *gyrAparCadeN*.

880

881 **Figure 5: LpsB and PbpG are imperative for the AdeN (GPN) and AdeL (GPL) mutants to**
882 **withstand Cip treatment.** (A) Transposon mutant fitness post Cip treatment at each insertion
883 position across the selected loci. (B) Growth of the indicated strains in the presence of Cip was
884 monitored as in Fig. 4, displayed as mean ± SD (n≥3). (C) Growth of deletion mutants in LB +
885 65 µg/ml Cip + 1mM IPTG to induce expression of the indicated genes complemented *in trans*
886 in GPN (column 2) or GPL (column 4) backgrounds. Data are means ± SEM (n≥6). Ciptx:
887 Ciprofloxacin treated. IPTG: Isopropyl β-d-1-thiogalactopyranoside. WT: wildtype. GP:
888 *gyrAparC.* GPL: *gyrAparCadeL*. GPN: *gyrAparCadeN*. EV: empty vector.

889

890 **Figure 6: The absence of either PbpG or LpsB results in reduced full-length LOS.** (A)
891 Extracts of noted strains were fractionated on Novex 16% tricine gel and stained with Pro-Q
892 Emerald 300 to reveal LOS. Representative images of three independent experiments are shown
893 (left). Quantification of gel fractionated LOS, normalized to total protein (right). Shown are

894 means relative to WT ± SD (n=3), individual LOS fractions in FQR strains vs in GP are
895 compared using two-way ANOVA with Dunnett's multiple comparisons (right). (A) Parent
896 strains. (B) *pbpG* deletion mutants. (C) *lpsB* deletion mutants. Significant differences are marked
897 with an asterisk, *=p-value of 0.0498. F: Full length LOS. I: Intermediate. U: Unspecified LMM
898 (low molecular mass) species. WT: wildtype. GPL: *gyrAparCadeL*. GPN: *gyrAparCadeN*. GPS:
899 *gyrAparCadeS*. GP: *gyrAparC*.

900

901 **Figure 7: Transcriptional and physiological response to pump overproduction.** (AB)
902 Alterations in intracellular pH (pHi) in response to pump overproduction. Noted strains grown to
903 mid-exponential phase in the absence (A) or presence (B) of Cip. Internal pH (pHi) was
904 measured using 20µM BCECF-AM as described (Materials and Methods). Displayed are the
905 means ± SEM for each strain from n=5-8 biological replicates, with P values derived from one-
906 way ANOVA making multiple comparisons. (C-F) Transcriptional alterations in response to
907 pump overproductions are magnified in presence of *adeL*ΔI335A336 mutation. Transcriptomic
908 data (n=3) was analyzed comparing high-level FQR pump hyper-expressing strains and the GP
909 parent strain (Materials and Methods). Differences in transcript levels for each comparison are
910 shown via the heat maps with GP vs GPL (C, +Cip) and (D, -Cip), GP vs GPN (E) and GP vs
911 GPS in (F). * = $p < 0.05$ (0.0259); ns=not significant. WT: wildtype. GPL: *gyrAparCadeL.* GPN:
912 *gyrAparCadeN*. GPS: *gyrAparCadeS*. GP: *gyrAparC*. Mid: mid-exponential phase. EPE: early
913 post-exponential phase.

914

915 **Figure 8: The presence of *adeL*ΔI335A336 in GPL results in overexpression of the *paa***
916 **operon.** RNA was isolated from GP and GPL strains and transcription of *paaA* gene was
917 quantified by q-rtPCR. Strains grown to exponential (A) or early post-exponential phase (B) in
918 absence of drug. Data are mean fold change in transcript levels ($2^{-\Delta\Delta CT}$) ± SEM of each target
919 (n=3) compared to parental GP strain, analyzed by two-tailed t test. Significance marked by
920 asterisks; **, p=0.0099; ***, p=0.0004. (C, D) Alterations in transcript levels in CRISPRi-
921 depleted *paaA* strain, with knockdown verified as described (Materials and Methods). RNA was
922 prepared from cultures grown to mid exponential (C) or early post-exponential phase (D). Data
923 are transcript levels of each target relative to nontargeting negative control ($2^{-\Delta\Delta CT}$) ± SEM
924 (n=3), analyzed by multiple unpaired t test analyses following the two-stage step-up Benjamini,
925 Krieger, and Yekutieli, false discovery rate of 5.00% (74). Significance: *, p=0.020-0.034; **,
926 p=0.002-0.003; ****, p<0.001. (E-G). Acidification of cytosol as a consequence of *paaA*
927 depletion. Internal pH (pHi) determined during mid-exponential phase in absence (E, F) or
928 presence (G) of Cip. (F). Intracellular pH in early post-exponential phase. Data are mean ± SEM
929 from n=5. P values were derived from an unpaired t test comparing the mean pHi values between
930 the two strains. (***, p<0.0009 in E) & (ns, p=0.8479 in F or 0.1821 in G). Untx: Untreated.
931 Ciptx: Ciprofloxacin treated at 30ug/mL. Mid: grown to mid-exponential phase. EPE: grown to
932 early post-exponential phase. GPL: *gyrAparCadeL*. GP: *gyrAparC*.

933

934 **Figure 9: *paaA* is significantly upregulated during Cip exposure.** (A,B) The *paaA* transcript
935 (shown with L2FCSE) is upregulated after Cip exposure independently of strain background.
936 Strains were grown to noted growth phases, with data derived from RNAseq experiments (Fig. 7;
937 Materials and Methods). Significance determined by s values from triplicate cultures for each (s

938 ≤ 1.11E-03). (C) Persistence of *adeL*ΔI335A336 single mutant (in WT strain background) is
939 unaffected by depletion of *paaA*. The indicated strains were grown to exponential phase with aTc
940 inducer to deplete *paaA* transcript, then exposed to Cip at ~20X MIC for the noted times prior to
941 plating on LB agar plates in absence of drug to determine CFU/mL. The mean CFU/mL ± SEM
942 are shown (n=3). The dotted line indicates LOD, the limit of detection for the assay (375
943 CFU/mL). Mid: grown to mid-exponential phase. EPE: grown to early post-exponential phase.
944 aTc: anhydrotetracycline. WT: wildtype. GPL: *gyrAparCadeL*. GPN: *gyrAparCadeN*. GPS:
945 *gyrAparCadeS*. GP: *gyrAparC*.

946

947 **Supplemental Figure 1.** CyoA-targeted KD causes a fitness defect. (A) Indicated strains grown
948 in LB broth + 100ng/mL aTc. A_{600} for culture density are displayed and their mean ± SEM (n=4-
949 5). *cyoA*-KD: strain harboring pWH1266 plasmid with *cyoA*-sgRNA vs NC-sgRNA is with
950 nontargeting sgRNA. (B) Culture samples harvested in exponential phase and transcript levels
951 determined by q-rtPCR (Materials and Methods). Displayed is mean fold change in transcript
952 levels ± SEM of each target compared to NC-sgRNA strain (n=3). (C) Read number plotted as
953 function of insertion site. Shown are: KD: knockdown. aTc: anhydrotetracycline. WT: wildtype.
954 GPL: *gyrAparCadeL*.

955

956 **Supplemental Figure 2.** OmpA, BfmS, LpsB, and PbpG are critical fitness determinants for
957 *adeL*ΔI335A336 strains during Cip exposure. Null mutants in FQR strain backgrounds compared
958 to the GP parent strain background. Growth was monitored every 15 minutes in 96 well plates.

959 Displayed are means ± SEM (n≥3). Ciptx: Ciprofloxacin treated. GP: *gyrAparC*. GPL:
960 *gyrAparCadeL*. GPN: *gyrAparCadeN*.

961

962 **Supplemental Figure 3.** Heatmaps of the normalized fitness of each transposon mutant in the
963 listed FQR strain and WT strain grown in indicated conditions relative to the fitness of the
964 population, alongside difference in fitness scores of the two strain backgrounds in that growth
965 condition (fitness in the high-level FQR strain – fitness in the WT drug susceptible parent).
966 Displayed are selected genes in which Tn10- and *Himar-1*-disruptions caused significantly
967 lowered fitness in the FQR strains in the absence or the presence of Cip (Significance described
968 in Materials and Methods). Gene names are followed by accession numbers which are preceded
969 by "NDEONHPJ_" per the ATCC 17978 strain annotations. Cip treated are those exposed to
970 Ciprofloxacin (Cip) at concentrations yielding 20-30% growth inhibition in each parent strain
971 compared to the untreated grown in parallel. WT: wildtype. GPL: *gyrAparCadeL*. GPN:
972 *gyrAparCadeN*. GPS: *gyrAparCadeS*.

973

974 **Supplemental Figure 4.** The observed minimum inhibitory concentrations (MIC) of Cip.
975 Growth conditions described in Fig. 4. A_{600} values are displayed with mean ± SEM shown (n≥3).
976 The observed MIC of Ciprofloxacin (Cip) for the indicated null mutation strains are exhibited as
977 relative to their parent strains' MIC (given a value of 1) (C). MIC exceeded this value
978 (arrowhead). WT: wildtype. GPL: *gyrAparCadeL*. GPN: *gyrAparCadeN*. GP: *gyrAparC*.

979

980 **Supplemental Figure 5: Nonadditive effects of overproducing two efflux pumps.** At least
981 three biological replicates of each strain were tested, all grown in LB with Ciprofloxacin
982 concentrations yielding comparable growth inhibition of the parent strains, 0.12µg/mL or
983 60µg/mL (A) or 0.14µg/mL (B). After growing to early post-exponential, all cultures were
984 diluted to A_{600}~0.003 in LB broth and culture density monitored every hour for five hours (A) or
985 every 15min overnight in a 96-well plate, though the first 8 hours are shown (B). Displayed is
986 the mean of the replicates ± SEM.

987

988

989

References

1. Peleg AY, Seifert H, Paterson DL. 2008. Acinetobacter baumannii: emergence of a successful pathogen. Clin Microbiol Rev 21:538-82.
2. CDC. 2019. Antibiotic Resistance Threats in the United States. Atlanta, GA: US Department of Health and Human Services, CDC.
3. CDC. 2022. COVID-19: U.S. Impact on Antimicrobial Resistance, Special Report 2022. Atlanta, GA: US Department of Health and Human Services, CDC.
4. Tomaras AP, Dorsey CW, Edelmann RE, Actis LA. 2003. Attachment to and biofilm formation on abiotic surfaces by Acinetobacter baumannii: involvement of a novel chaperone-usher pili assembly system. Microbiology (Reading) 149:3473-3484.
5. Badave GK, Kulkarni D. 2015. Biofilm Producing Multidrug Resistant Acinetobacter baumannii: An Emerging Challenge. J Clin Diagn Res 9:DC08-10.
6. Sanchez CJ, Jr., Mende K, Beckius ML, Akers KS, Romano DR, Wenke JC, Murray CK. 2013. Biofilm formation by clinical isolates and the implications in chronic infections. BMC Infect Dis 13:47.
7. Gonzalez-Villoria AM, Valverde-Garduno V. 2016. Antibiotic-Resistant Acinetobacter baumannii Increasing Success Remains a Challenge as a Nosocomial Pathogen. J Pathog 2016:7318075.
8. Tacconelli E, Carrara E, Savoldi A, Harbarth S, Mendelson M, Monnet DL, Pulcini C, Kahlmeter G, Kluytmans J, Carmeli Y, Ouellette M, Outterson K, Patel J, Cavaleri M, Cox EM, Houchens CR, Grayson ML, Hansen P, Singh N, Theuretzbacher U, Magrini N, Group WHOPPLW. 2018. Discovery, research, and development of new antibiotics: the WHO priority list of antibiotic-resistant bacteria and tuberculosis. Lancet Infect Dis 18:318-327.
9. Lob SH, Hoban DJ, Sahm DF, Badal RE. 2016. Regional differences and trends in antimicrobial susceptibility of Acinetobacter baumannii. Int J Antimicrob Agents 47:317-23.
10. Giammanco A, Cala C, Fasciana T, Dowzicky MJ. 2017. Global Assessment of the Activity of Tigecycline against Multidrug-Resistant Gram-Negative Pathogens between 2004 and 2014 as Part of the Tigecycline Evaluation and Surveillance Trial. mSphere 2.
11. Poole K. 2004. Efflux-mediated multiresistance in Gram-negative bacteria. Clin Microbiol Infect 10:12-26.
12. Sun J, Deng Z, Yan A. 2014. Bacterial multidrug efflux pumps: mechanisms, physiology and pharmacological exploitations. Biochem Biophys Res Commun 453:254-67.
13. Coyne S, Courvalin P, Perichon B. 2011. Efflux-mediated antibiotic resistance in Acinetobacter spp. Antimicrob Agents Chemother 55:947-53.
14. Blair JM, Webber MA, Baylay AJ, Ogbolu DO, Piddock LJ. 2015. Molecular mechanisms of antibiotic resistance. Nat Rev Microbiol 13:42-51.
15. Geisinger E, Huo W, Hernandez-Bird J, Isberg RR. 2019. Acinetobacter baumannii: Envelope Determinants That Control Drug Resistance, Virulence, and Surface Variability. Annu Rev Microbiol 73:481-506.
16. Compagne N, Vieira Da Cruz A, Muller RT, Hartkoorn RC, Flipo M, Pos KM. 2023. Update on the Discovery of Efflux Pump Inhibitors against Critical Priority Gram-Negative Bacteria. Antibiotics (Basel) 12.
17. Geisinger E, Vargas-Cuebas G, Mortman NJ, Syal S, Dai Y, Wainwright EL, Lazinski D, Wood S, Zhu Z, Anthony J, van Opijnen T, Isberg RR. 2019. The Landscape of Phenotypic and Transcriptional Responses to Ciprofloxacin in Acinetobacter baumannii: Acquired Resistance Alleles Modulate Drug-Induced SOS Response and Prophage Replication. mBio 10.

1035 18. Naidu V, Bartczak A, Brzoska AJ, Lewis P, Eijkelkamp BA, Paulsen IT, Elbourne LDH, Hassan KA.
1036 2023. Evolution of RND efflux pumps in the development of a successful pathogen. Drug Resist
1037 Updat 66:100911.
1038 19. Pagdepanichkit S, Tribuddharat C, Chuanchuen R. 2016. Distribution and expression of the Ade
1039 multidrug efflux systems in Acinetobacter baumannii clinical isolates. Can J Microbiol 62:794-
1040 801.
1041 20. Magnet S, Courvalin P, Lambert T. 2001. Resistance-nodulation-cell division-type efflux pump
1042 involved in aminoglycoside resistance in Acinetobacter baumannii strain BM4454. Antimicrob
1043 Agents Chemother 45:3375-80.
1044 21. Coyne S, Rosenfeld N, Lambert T, Courvalin P, Perichon B. 2010. Overexpression of resistance-
1045 nodulation-cell division pump AdeFGH confers multidrug resistance in Acinetobacter baumannii.
1046 Antimicrob Agents Chemother 54:4389-93.
1047 22. Yoon EJ, Chabane YN, Goussard S, Snesrud E, Courvalin P, De E, Grillot-Courvalin C. 2015.
1048 Contribution of resistance-nodulation-cell division efflux systems to antibiotic resistance and
1049 biofilm formation in Acinetobacter baumannii. mBio 6.
1050 23. Rosenfeld N, Bouchier C, Courvalin P, Perichon B. 2012. Expression of the resistance-nodulation-
1051 cell division pump AdeIJK in Acinetobacter baumannii is regulated by AdeN, a TetR-type
1052 regulator. Antimicrob Agents Chemother 56:2504-10.
1053 24. Anonymous. !!! INVALID CITATION !!! [Wang, 2017 #4060;Wang, 2017 #4060;Murakami, 2002
1054 #4054].
1055 25. Murakami S, Nakashima R, Yamashita E, Yamaguchi A. 2002. Crystal structure of bacterial
1056 multidrug efflux transporter AcrB. Nature 419:587-93.
1057 26. Murakami S, Nakashima R, Yamashita E, Matsumoto T, Yamaguchi A. 2006. Crystal structures of
1058 a multidrug transporter reveal a functionally rotating mechanism. Nature 443:173-9.
1059 27. Koronakis V, Sharff A, Koronakis E, Luisi B, Hughes C. 2000. Crystal structure of the bacterial
1060 membrane protein TolC central to multidrug efflux and protein export. Nature 405:914-9.
1061 28. Yu EW, Aires JR, McDermott G, Nikaido H. 2005. A periplasmic drug-binding site of the AcrB
1062 multidrug efflux pump: a crystallographic and site-directed mutagenesis study. J Bacteriol
1063 187:6804-15.
1064 29. Yu EW, McDermott G, Zgurskaya HI, Nikaido H, Koshland DE, Jr. 2003. Structural basis of
1065 multiple drug-binding capacity of the AcrB multidrug efflux pump. Science 300:976-80.
1066 30. Higgins MK, Bokma E, Koronakis E, Hughes C, Koronakis V. 2004. Structure of the periplasmic
1067 component of a bacterial drug efflux pump. Proc Natl Acad Sci U S A 101:9994-9.
1068 31. DeJesus MA, Ambadipudi C, Baker R, Sassetti C, Ioerger TR. 2015. TRANSIT--A Software Tool for
1069 Himar1 TnSeq Analysis. PLoS Comput Biol 11:e1004401.
1070 32. Arai H, Kawakami T, Osamura T, Hirai T, Sakai Y, Ishii M. 2014. Enzymatic characterization and in
1071 vivo function of five terminal oxidases in Pseudomonas aeruginosa. J Bacteriol 196:4206-15.
1072 33. Borisov VB, Verkhovsky MI. 2015. Oxygen as Acceptor. EcoSal Plus 6.
1073 34. van Opijnen T, Bodi KL, Camilli A. 2009. Tn-seq: high-throughput parallel sequencing for fitness
1074 and genetic interaction studies in microorganisms. Nat Methods 6:767-72.
1075 35. Geisinger E, Mortman NJ, Dai Y, Cokol M, Syal S, Farinha A, Fisher DG, Tang AY, Lazinski DW,
1076 Wood S, Anthony J, van Opijnen T, Isberg RR. 2020. Antibiotic susceptibility signatures identify
1077 potential antimicrobial targets in the Acinetobacter baumannii cell envelope. Nat Commun
1078 11:4522.
1079 36. Geisinger E, Mortman NJ, Vargas-Cuebas G, Tai AK, Isberg RR. 2018. A global regulatory system
1080 links virulence and antibiotic resistance to envelope homeostasis in Acinetobacter baumannii.
1081 PLoS Pathog 14:e1007030.

1082 37. Nikaido H, Takatsuka Y. 2009. Mechanisms of RND multidrug efflux pumps. Biochim Biophys
1083 Acta 1794:769-81.
1084 38. Teufel R, Mascaraque V, Ismail W, Voss M, Perera J, Eisenreich W, Haehnel W, Fuchs G. 2010.
1085 Bacterial phenylalanine and phenylacetate catabolic pathway revealed. Proc Natl Acad Sci U S A
1086 107:14390-5.
1087 39. Hooppaw AJ, McGuffey JC, Di Venanzio G, Ortiz-Marquez JC, Weber BS, Lightly TJ, van Opijnen T,
1088 Scott NE, Cardona ST, Feldman MF. 2022. The Phenylacetic Acid Catabolic Pathway Regulates
1089 Antibiotic and Oxidative Stress Responses in Acinetobacter. mBio 13:e0186321.
1090 40. Green ER, Juttukonda LJ, Skaar EP. 2020. The Manganese-Responsive Transcriptional Regulator
1091 MumR Protects Acinetobacter baumannii from Oxidative Stress. Infect Immun 88.
1092 41. Vega NM, Allison KR, Khalil AS, Collins JJ. 2012. Signaling-mediated bacterial persister formation.
1093 Nat Chem Biol 8:431-3.
1094 42. Wu Y, Vulic M, Keren I, Lewis K. 2012. Role of oxidative stress in persister tolerance. Antimicrob
1095 Agents Chemother 56:4922-6.
1096 43. Lee HH, Molla MN, Cantor CR, Collins JJ. 2010. Bacterial charity work leads to population-wide
1097 resistance. Nature 467:82-5.
1098 44. Huo W, Busch LM, Hernandez-Bird J, Hamami E, Marshall CW, Geisinger E, Cooper VS, van
1099 Opijnen T, Rosch JW, Isberg RR. 2022. Immunosuppression broadens evolutionary pathways to
1100 drug resistance and treatment failure during Acinetobacter baumannii pneumonia in mice. Nat
1101 Microbiol 7:796-809.
1102 45. Law RJ, Hamlin JN, Sivro A, McCorrister SJ, Cardama GA, Cardona ST. 2008. A functional
1103 phenylacetic acid catabolic pathway is required for full pathogenicity of Burkholderia
1104 cenocepacia in the Caenorhabditis elegans host model. J Bacteriol 190:7209-18.
1105 46. Musthafa KS, Sivamaruthi BS, Pandian SK, Ravi AV. 2012. Quorum sensing inhibition in
1106 Pseudomonas aeruginosa PAO1 by antagonistic compound phenylacetic acid. Curr Microbiol
1107 65:475-80.
1108 47. Lightly TJ, Frejuk KL, Groleau MC, Chiarelli LR, Ras C, Buroni S, Deziel E, Sorensen JL, Cardona ST.
1109 2019. Phenylacetyl Coenzyme A, Not Phenylacetic Acid, Attenuates CepIR-Regulated Virulence in
1110 Burkholderia cenocepacia. Appl Environ Microbiol 85.
1111 48. Park JS, Lee WC, Yeo KJ, Ryu KS, Kumarasiri M, Hesek D, Lee M, Mobashery S, Song JH, Kim SI,
1112 Lee JC, Cheong C, Jeon YH, Kim HY. 2012. Mechanism of anchoring of OmpA protein to the cell
1113 wall peptidoglycan of the gram-negative bacterial outer membrane. FASEB J 26:219-28.
1114 49. Gribun A, Nitzan Y, Pechatnikov I, Hershkovits G, Katcoff DJ. 2003. Molecular and structural
1115 characterization of the HMP-AB gene encoding a pore-forming protein from a clinical isolate of
1116 Acinetobacter baumannii. Curr Microbiol 47:434-43.
1117 50. Sugawara E, Nikaido H. 2012. OmpA is the principal nonspecific slow porin of Acinetobacter
1118 baumannii. J Bacteriol 194:4089-96.
1119 51. Iyer R, Moussa SH, Durand-Reville TF, Tommasi R, Miller A. 2018. Acinetobacter baumannii
1120 OmpA Is a Selective Antibiotic Permeant Porin. ACS Infect Dis 4:373-381.
1121 52. Kim SY, Kim MH, Kim SI, Son JH, Kim S, Lee YC, Shin M, Oh MH, Lee JC. 2019. The sensor kinase
1122 BfmS controls production of outer membrane vesicles in Acinetobacter baumannii. BMC
1123 Microbiol 19:301.
1124 53. Moon DC, Choi CH, Lee JH, Choi CW, Kim HY, Park JS, Kim SI, Lee JC. 2012. Acinetobacter
1125 baumannii outer membrane protein A modulates the biogenesis of outer membrane vesicles. J
1126 Microbiol 50:155-60.
1127 54. Simpson BW, Nieckarz M, Pinedo V, McLean AB, Cava F, Trent MS. 2021. Acinetobacter
1128 baumannii Can Survive with an Outer Membrane Lacking Lipooligosaccharide Due to Structural
1129 Support from Elongasome Peptidoglycan Synthesis. mBio 12:e0309921.

1130 55. Xu Y, Moeller A, Jun SY, Le M, Yoon BY, Kim JS, Lee K, Ha NC. 2012. Assembly and channel
1131 opening of outer membrane protein in tripartite drug efflux pumps of Gram-negative bacteria. J
1132 Biol Chem 287:11740-50.
1133 56. Ma M, Lustig M, Salem M, Mengin-Lecreulx D, Phan G, Broutin I. 2021. MexAB-OprM Efflux
1134 Pump Interaction with the Peptidoglycan of Escherichia coli and Pseudomonas aeruginosa. Int J
1135 Mol Sci 22.
1136 57. Arunmanee W, Pathania M, Solovyova AS, Le Brun AP, Ridley H, Basle A, van den Berg B, Lakey
1137 JH. 2016. Gram-negative trimeric porins have specific LPS binding sites that are essential for
1138 porin biogenesis. Proc Natl Acad Sci U S A 113:E5034-43.
1139 58. Webby MN, Oluwole AO, Pedebos C, Inns PG, Olerinyova A, Prakaash D, Housden NG, Benn G,
1140 Sun D, Hoogenboom BW, Kukura P, Mohammed S, Robinson CV, Khalid S, Kleanthous C. 2022.
1141 Lipids mediate supramolecular outer membrane protein assembly in bacteria. Sci Adv
1142 8:eadc9566.
1143 59. Gwin CM, Prakash N, Christian Belisario J, Haider L, Rosen ML, Martinez LR, Rigel NW. 2018. The
1144 apolipoprotein N-acyl transferase Lnt is dispensable for growth in Acinetobacter species.
1145 Microbiology (Reading) 164:1547-1556.
1146 60. Powers MJ, Trent MS. 2018. Phospholipid retention in the absence of asymmetry strengthens
1147 the outer membrane permeability barrier to last-resort antibiotics. Proc Natl Acad Sci U S A
1148 115:E8518-E8527.
1149 61. Boll JM, Tucker AT, Klein DR, Beltran AM, Brodbelt JS, Davies BW, Trent MS. 2015. Reinforcing
1150 Lipid A Acylation on the Cell Surface of Acinetobacter baumannii Promotes Cationic
1151 Antimicrobial Peptide Resistance and Desiccation Survival. mBio 6:e00478-15.
1152 62. Bhuiyan MS, Ellett F, Murray GL, Kostoulias X, Cerqueira GM, Schulze KE, Mahamad Maifiah MH,
1153 Li J, Creek DJ, Lieschke GJ, Peleg AY. 2016. Acinetobacter baumannii phenylacetic acid
1154 metabolism influences infection outcome through a direct effect on neutrophil chemotaxis. Proc
1155 Natl Acad Sci U S A 113:9599-604.
1156 63. Wang J, Dong Y, Zhou T, Liu X, Deng Y, Wang C, Lee J, Zhang LH. 2013. Pseudomonas aeruginosa
1157 cytotoxicity is attenuated at high cell density and associated with the accumulation of
1158 phenylacetic acid. PLoS One 8:e60187.
1159 64. Geisinger E, Isberg RR. 2015. Antibiotic modulation of capsular exopolysaccharide and virulence
1160 in Acinetobacter baumannii. PLoS Pathog 11:e1004691.
1161 65. Gomori S. 1995. Meth Enzymol 1:143.
1162 66. Clementi EA, Marks LR, Roche-Hakansson H, Hakansson AP. 2014. Monitoring changes in
1163 membrane polarity, membrane integrity, and intracellular ion concentrations in Streptococcus
1164 pneumoniae using fluorescent dyes. J Vis Exp doi:10.3791/51008:e51008.
1165 67. McCoy KM, Antonio ML, van Opijnen T. 2017. MAGenTA: a Galaxy implemented tool for
1166 complete Tn-Seq analysis and data visualization. Bioinformatics 33:2781-2783.
1167 68. Jensen PA, Zhu Z, van Opijnen T. 2017. Antibiotics Disrupt Coordination between Transcriptional
1168 and Phenotypic Stress Responses in Pathogenic Bacteria. Cell Rep 20:1705-1716.
1169 69. Zhu Z, Surujon D, Ortiz-Marquez JC, Huo W, Isberg RR, Bento J, van Opijnen T. 2020. Entropy of a
1170 bacterial stress response is a generalizable predictor for fitness and antibiotic sensitivity. Nat
1171 Commun 11:4365.
1172 70. Shishkin AA, Giannoukos G, Kucukural A, Ciulla D, Busby M, Surka C, Chen J, Bhattacharyya RP,
1173 Rudy RF, Patel MM, Novod N, Hung DT, Gnirke A, Garber M, Guttman M, Livny J. 2015.
1174 Simultaneous generation of many RNA-seq libraries in a single reaction. Nat Methods 12:323-5.
1175 71. Huang Y, Sheth RU, Kaufman A, Wang HH. 2020. Scalable and cost-effective ribonuclease-based
1176 rRNA depletion for transcriptomics. Nucleic Acids Res 48:e20.

1177 72. Martin M. 2011. Cutadapt removes adapter sequences from high-throughput sequencing reads.
1178 2011 17:3.
1179 73. Benjamini Y, & Hochberg, Y. 1995. Controlling the false discovery rate: a practical and powerful
1180 approach to multiple testing. Journal of the Royal Statistical Society Series B
1181 (Methodological):289-300.
1182 74. Benjamini Y, Krieger, A. M., & Yekutieli, D. 2006. Adaptive linear step-up procedures that control
1183 the false discovery rate. Biometrika 93:491-507.

1184

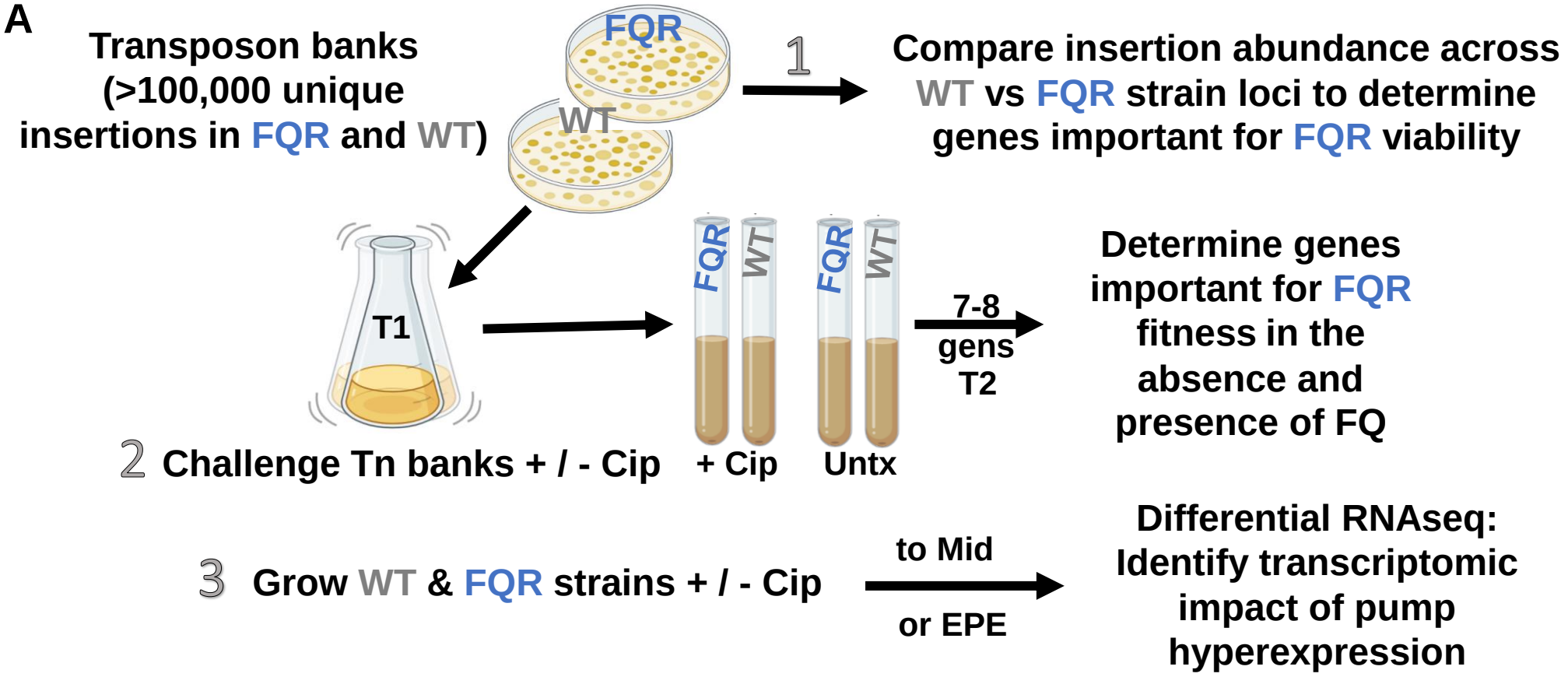
A
Transposon banks (>100,000 unique insertions in FQR and WT)
FQR
WT
1
Compare insertion abundance across WT vs FQR strain loci to determine genes important for FQR viability
T1
FQR
WT
FQR
WT
7-8 gens T2
Determine genes important for FQR fitness in the absence and presence of FQ
2 Challenge Tn banks + / - Cip
+ Cip
Untx
3 Grow WT & FQR strains + / - Cip
to Mid
or EPE
Differential RNAseq: Identify transcriptomic impact of pump hyperexpression

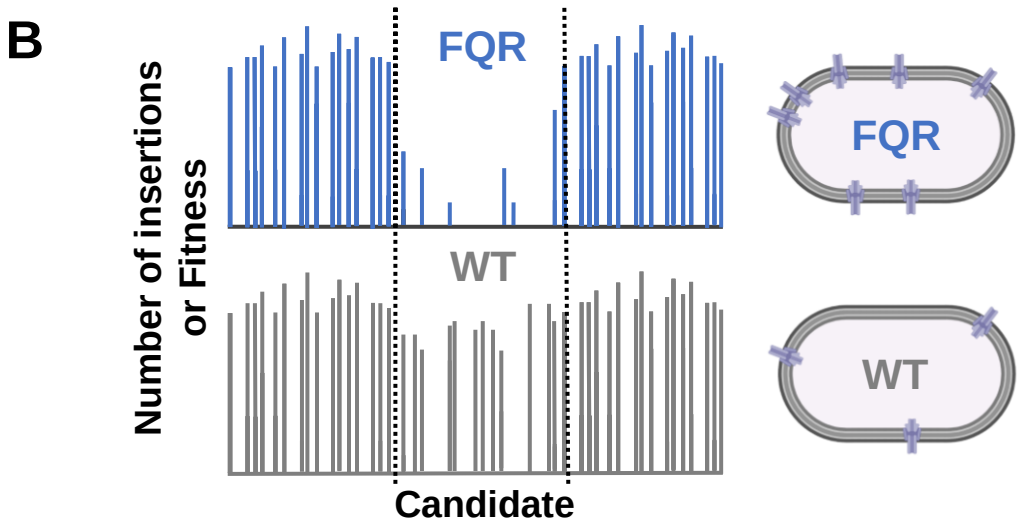
B
FQR
WT
Number of insertions or Fitness
Candidate
FQR
WT

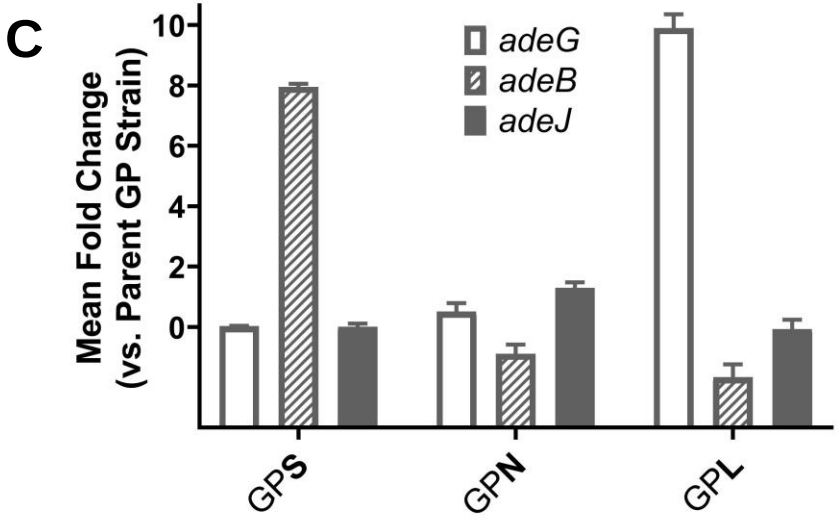
C
Mean Fold Change (vs. Parent GP Strain)
10
8
6
4
2
0
adeG
adeB
adeJ
GPS
GPN
GPL

Fig1

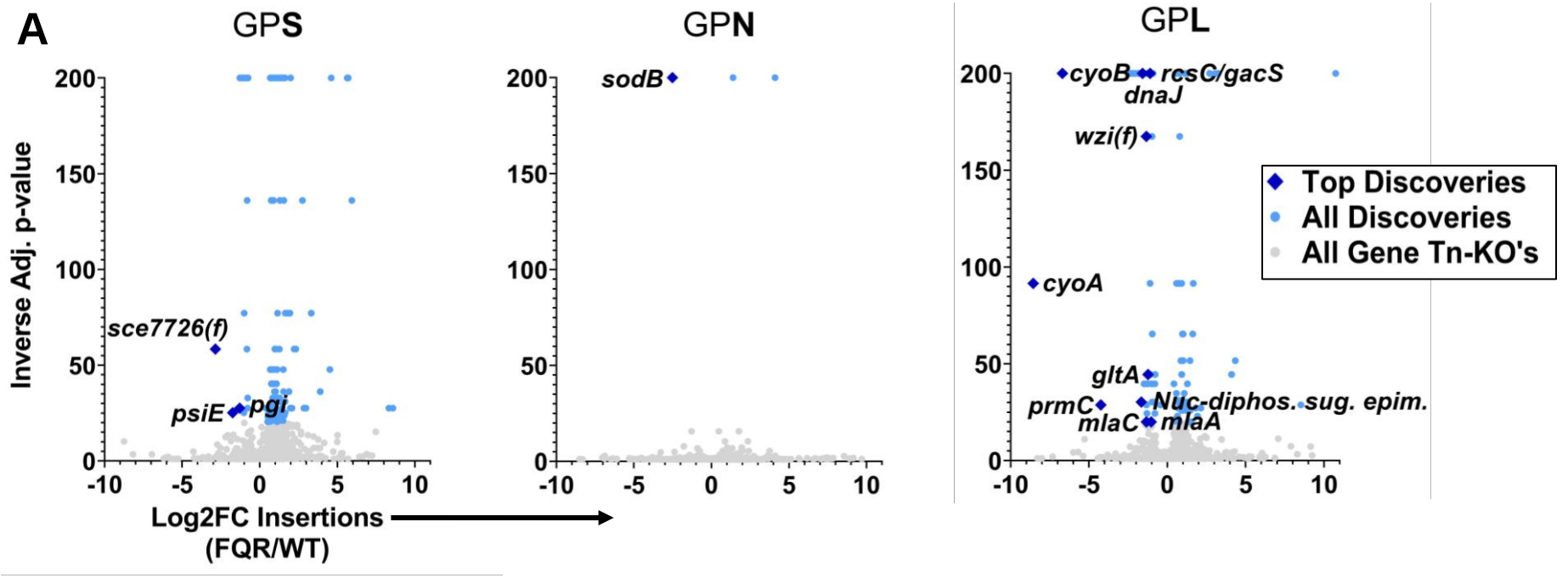
A
GPS
GPN
GPL
Inverse Adj. p-value
Log2FC Insertions
(FQR/WT)
sce7726(f)
psiE
pgi
sodB
cyoB
rcsC/gacS
dnaJ
wzi(f)
cyoA
gltA
prmC
mlaC
mlaA
Nuc-diphos. sug. epim.
Top Discoveries
All Discoveries
All Gene Tn-KO's

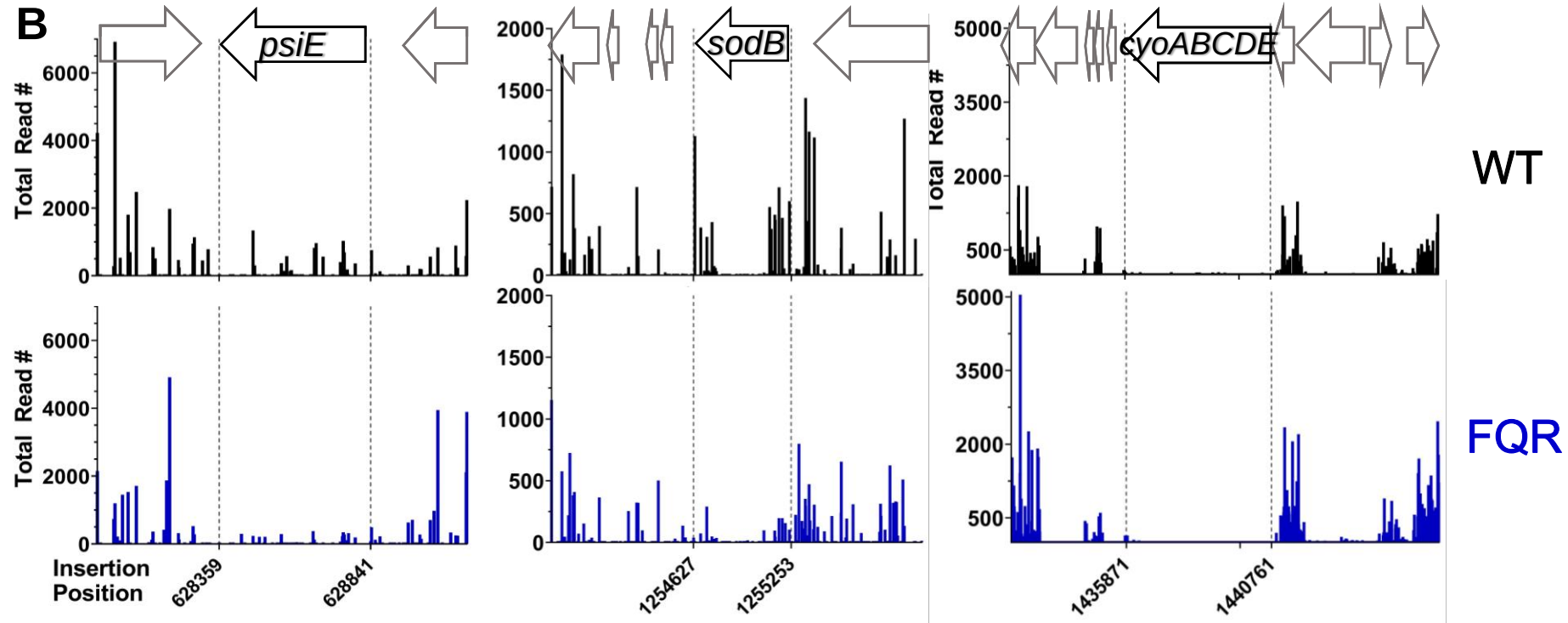
B
psiE
sodB
cyoABCDE
Total Read #
WT
FQR
Insertion
Position
628359
628841
1254627
1255253
1435871
1440761

Fig 2

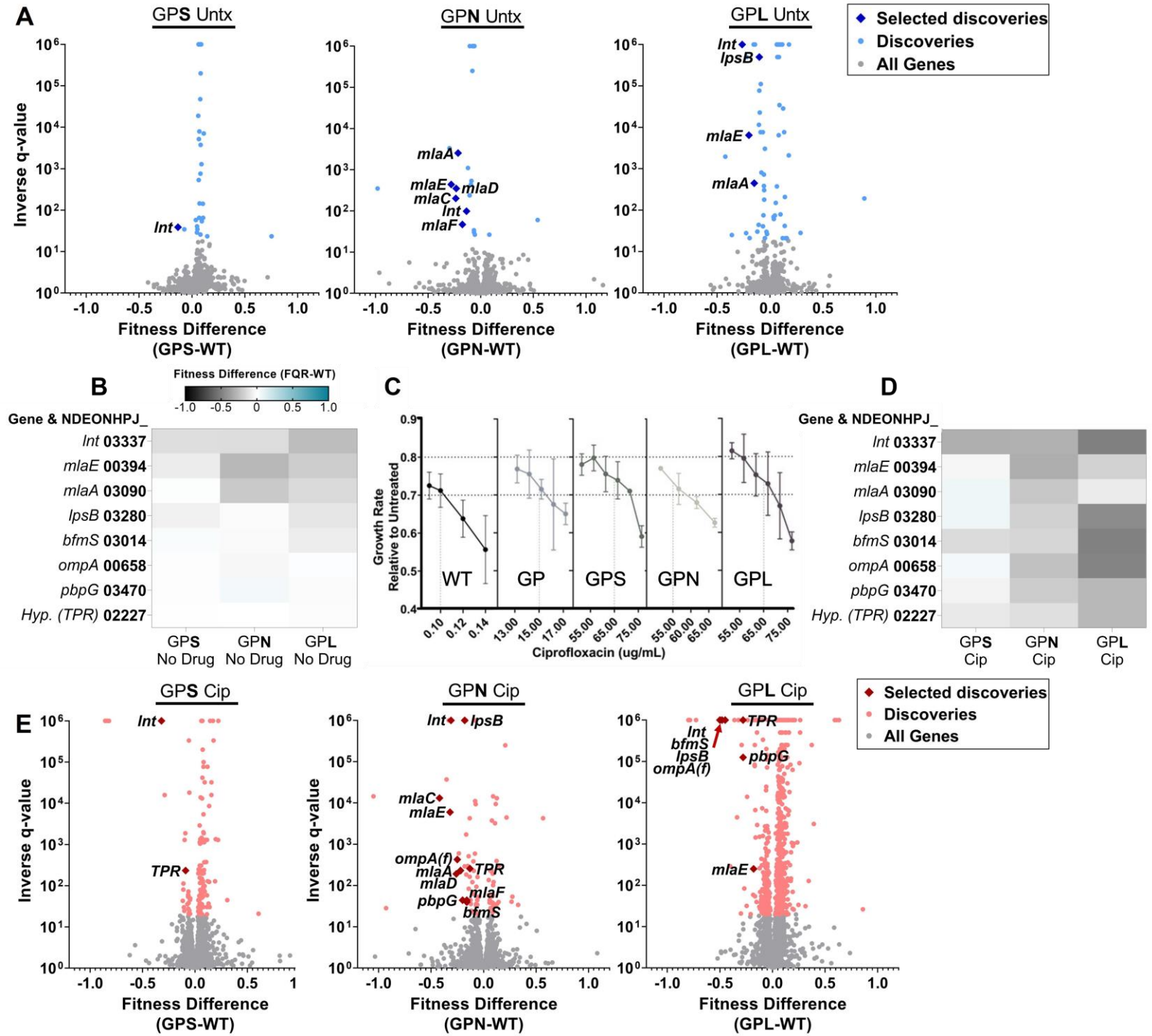
A
GPS Untx
GPN Untx
GPL Untx
Selected discoveries
Discoveries
All Genes
Inverse q-value
Fitness Difference (GPS-WT)
Fitness Difference (GPN-WT)
Fitness Difference (GPL-WT)
Int
mlaA
mlaE
mlaD
mlaC
mlaF
lpsB
B
Fitness Difference (FQR-WT)
Gene & NDEONHPJ_
Int 03337
mlaE 00394
mlaA 03090
lpsB 03280
bfmS 03014
ompA 00658
pbpG 03470
Hyp. (TPR) 02227
GPS No Drug
GPN No Drug
GPL No Drug
C
Growth Rate Relative to Untreated
WT
GP
GPS
GPN
GPL
Ciprofloxacin (ug/mL)
D
GPS Cip
GPN Cip
GPL Cip
E
GPS Cip
GPN Cip
GPL Cip
TPR
ompA(f)

Fig 3

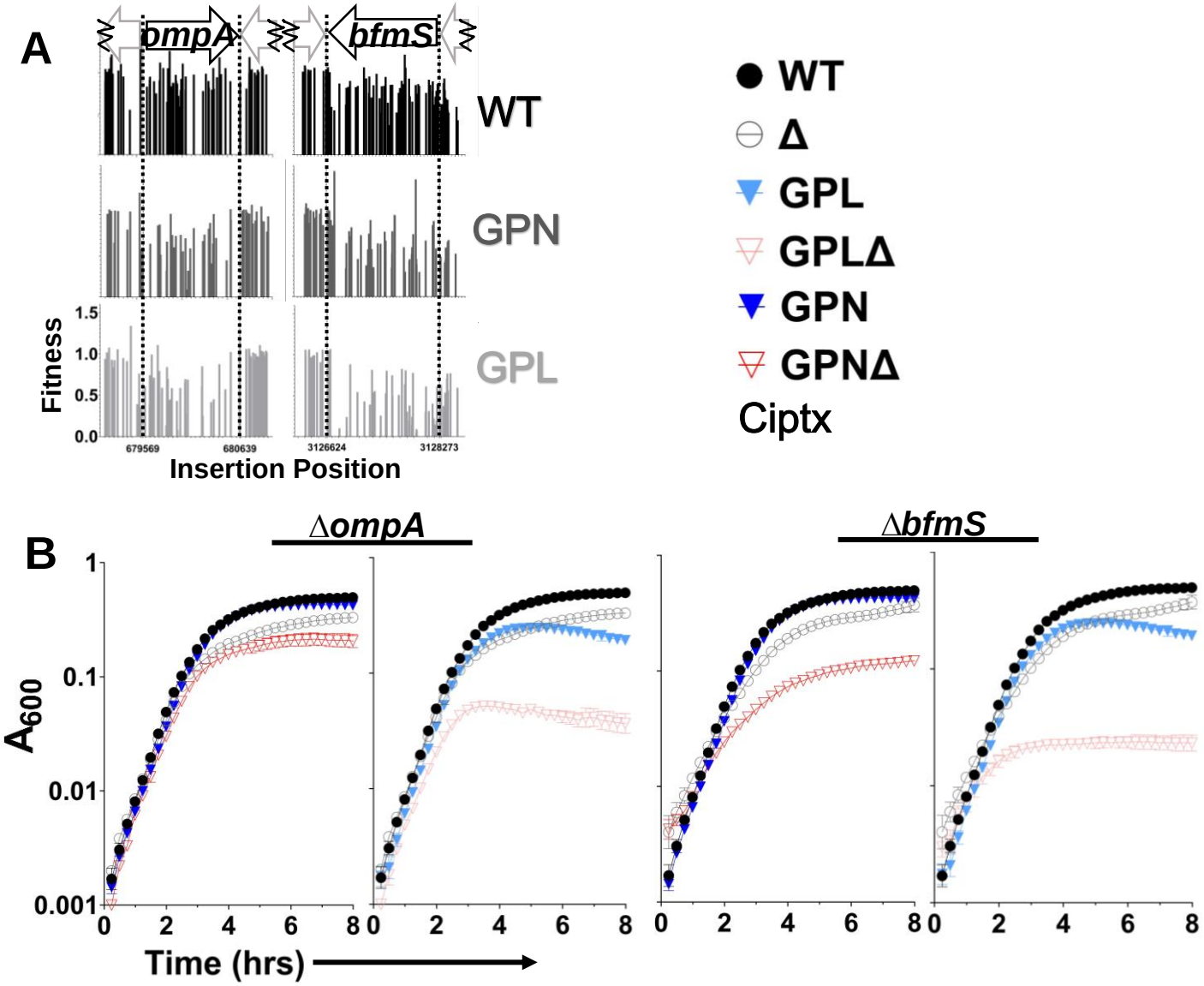
A
ompA
bfmS
WT
GPN
GPL
Fitness
1.5
1.0
0.5
0.0
679569
680639
3126624
3128273
Insertion Position
WT
Δ
GPL
GPLΔ
GPN
GPNΔ
Ciptx
B
ΔompA
ΔbfmS
A600
1
0.1
0.01
0.001
0
2
4
6
8
Time (hrs)

Fig. 4

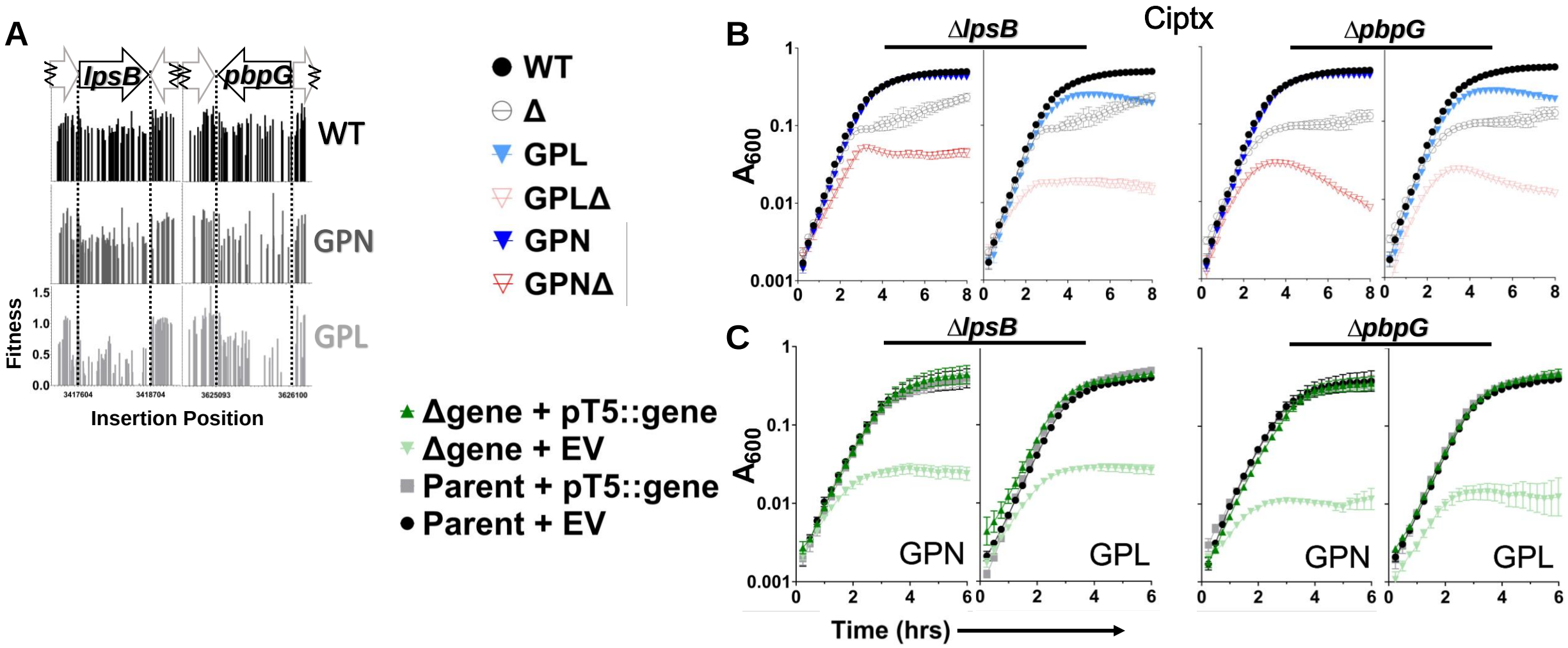
A
lpsB
pbpG
WT
GPN
GPL
Fitness
1.5
1.0
0.5
0.0
3417604
3418704
3625093
3626100
Insertion Position
WT
Δ
GPL
GPLΔ
GPN
GPNΔ
Δgene + pT5::gene
Δgene + EV
Parent + pT5::gene
Parent + EV
B
Ciptx
ΔlpsB
ΔpbpG
A600
1
0.1
0.01
0.001
0
2
4
6
8
C
GPN
GPL
Time (hrs)

Fig. 5

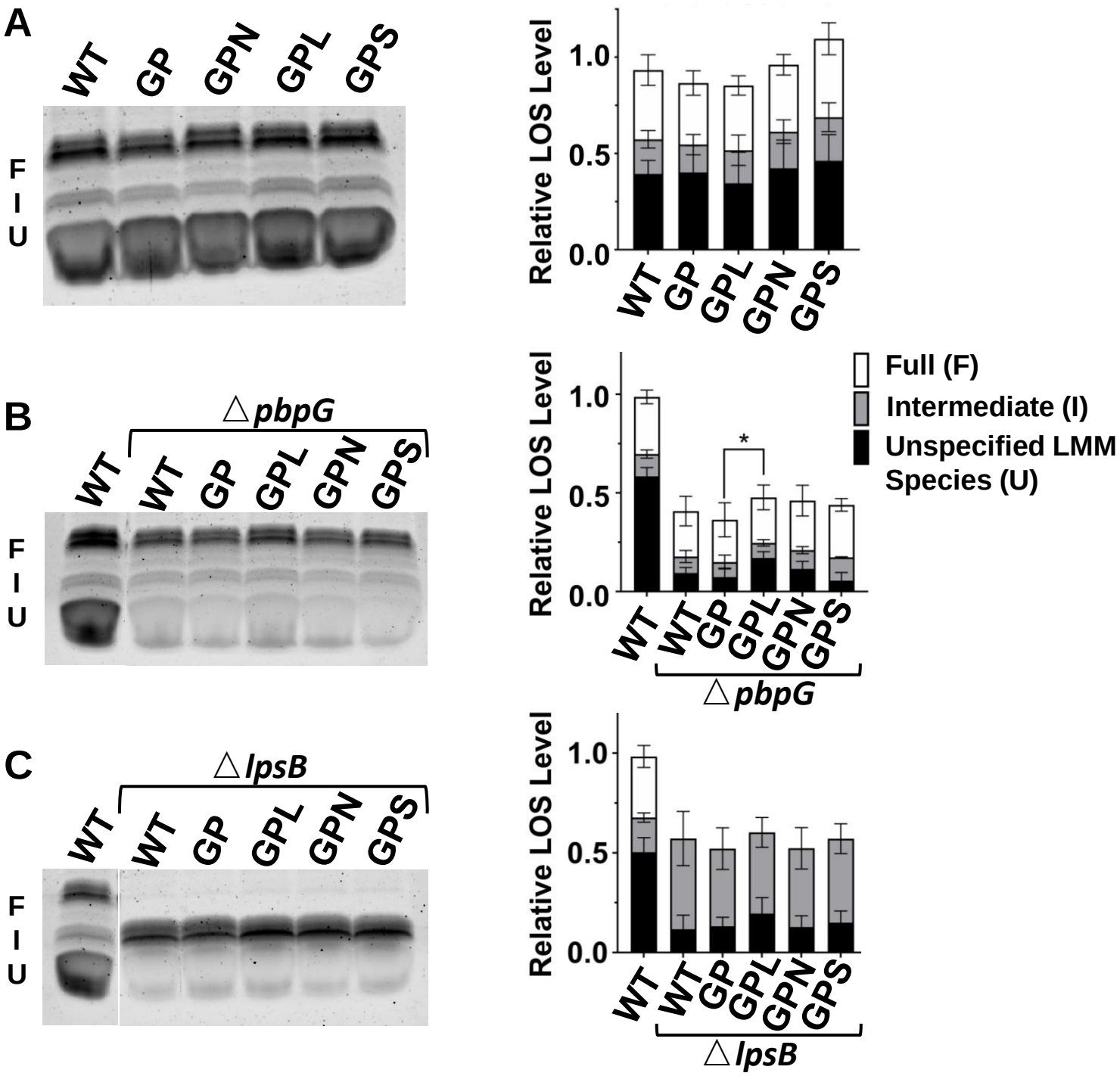
A
WT
GP
GPN
GPL
GPS
F
I
U
Relative LOS Level
1.0
0.5
0.0
B
△pbpG
C
△lpsB
*
Full (F)
Intermediate (I)
Unspecified LMM Species (U)

Fig. 6

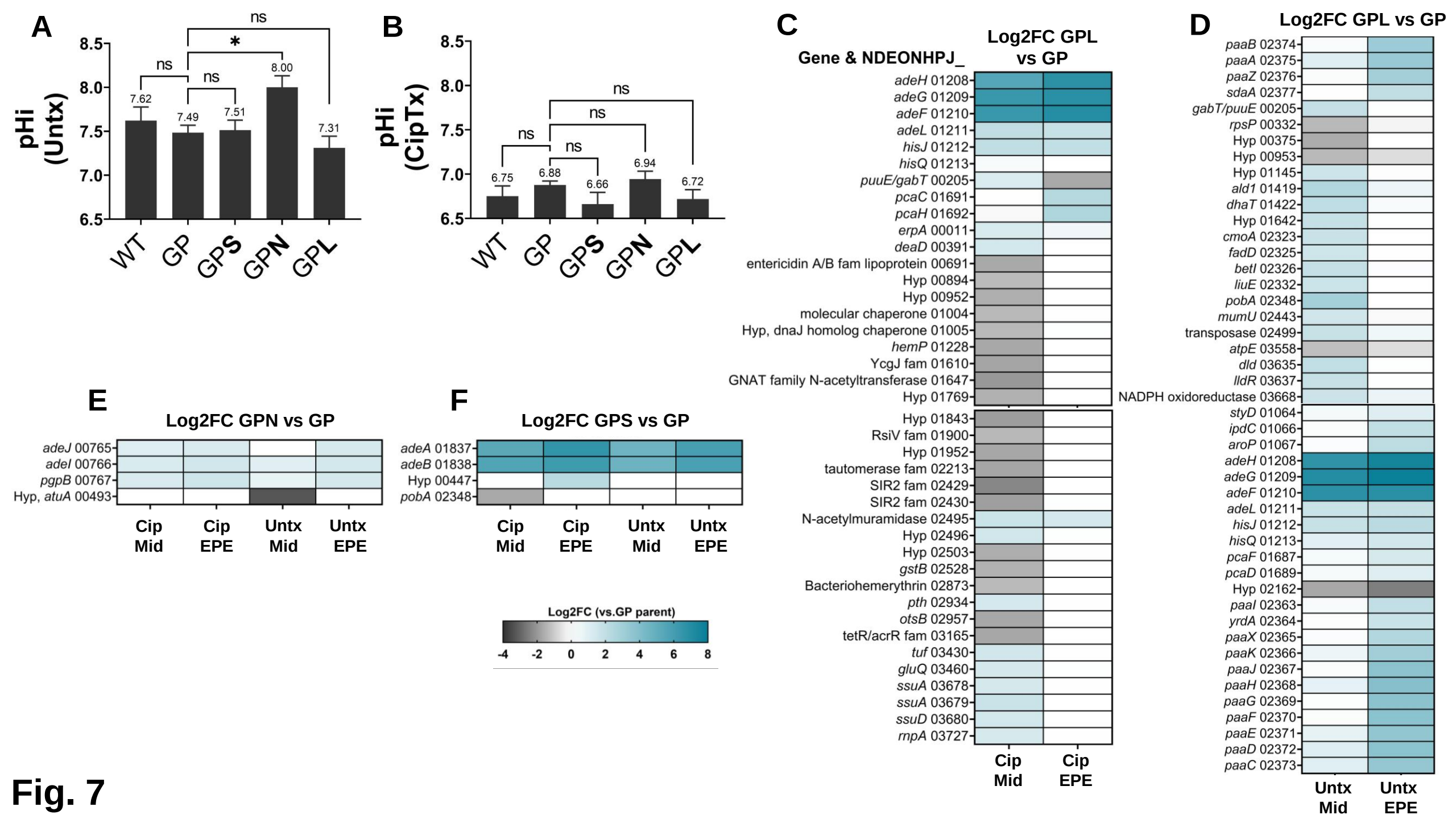
A
pHi (Untx)
8.5
8.0
7.5
7.0
6.5
ns
*
ns
ns
7.62
7.49
7.51
8.00
7.31
WT
GP
GPS
GPN
GPL
B
pHi (CipTx)
ns
ns
ns
ns
6.75
6.88
6.66
6.94
6.72
WT
GP
GPS
GPN
GPL
C
Gene & NDEONHPJ_
Log2FC GPL vs GP
adeH 01208
adeG 01209
adeF 01210
adeL 01211
hisJ 01212
hisQ 01213
puuE/gabT 00205
pcaC 01691
pcaH 01692
erpA 00011
deaD 00391
entericidin A/B fam lipoprotein 00691
Hyp 00894
Hyp 00952
molecular chaperone 01004
Hyp, dnaJ homolog chaperone 01005
hemP 01228
YcgJ fam 01610
GNAT family N-acetyltransferase 01647
Hyp 01769
Hyp 01843
RsiV fam 01900
Hyp 01952
tautomerase fam 02213
SIR2 fam 02429
SIR2 fam 02430
N-acetylmuramidase 02495
Hyp 02496
Hyp 02503
gstB 02528
Bacteriohemerythrin 02873
pth 02934
otsB 02957
tetR/acrR fam 03165
tuf 03430
gluQ 03460
ssuA 03678
ssuA 03679
ssuD 03680
rnpA 03727
Cip Mid
Cip EPE
D
Log2FC GPL vs GP
paaB 02374
paaA 02375
paaZ 02376
sdaA 02377
gabT/puuE 00205
rpsP 00332
Hyp 00375
Hyp 00953
Hyp 01145
ald1 01419
dhaT 01422
Hyp 01642
cmoA 02323
fadD 02325
betI 02326
liuE 02332
pobA 02348
mumU 02443
transposase 02499
atpE 03558
dld 03635
lldR 03637
NADPH oxidoreductase 03668
styD 01064
ipdC 01066
aroP 01067
adeH 01208
adeG 01209
adeF 01210
adeL 01211
hisJ 01212
hisQ 01213
pcaF 01687
pcaD 01689
Hyp 02162
paaI 02363
yrdA 02364
paaX 02365
paaK 02366
paaJ 02367
paaH 02368
paaG 02369
paaF 02370
paaE 02371
paaD 02372
paaC 02373
Untx Mid
Untx EPE
E
Log2FC GPN vs GP
adeJ 00765
adeI 00766
pgpB 00767
Hyp, atuA 00493
Cip Mid
Cip EPE
Untx Mid
Untx EPE
F
Log2FC GPS vs GP
adeA 01837
adeB 01838
Hyp 00447
pobA 02348
Cip Mid
Cip EPE
Untx Mid
Untx EPE
Log2FC (vs.GP parent)
-4
-2
0
2
4
6
8

Fig. 7

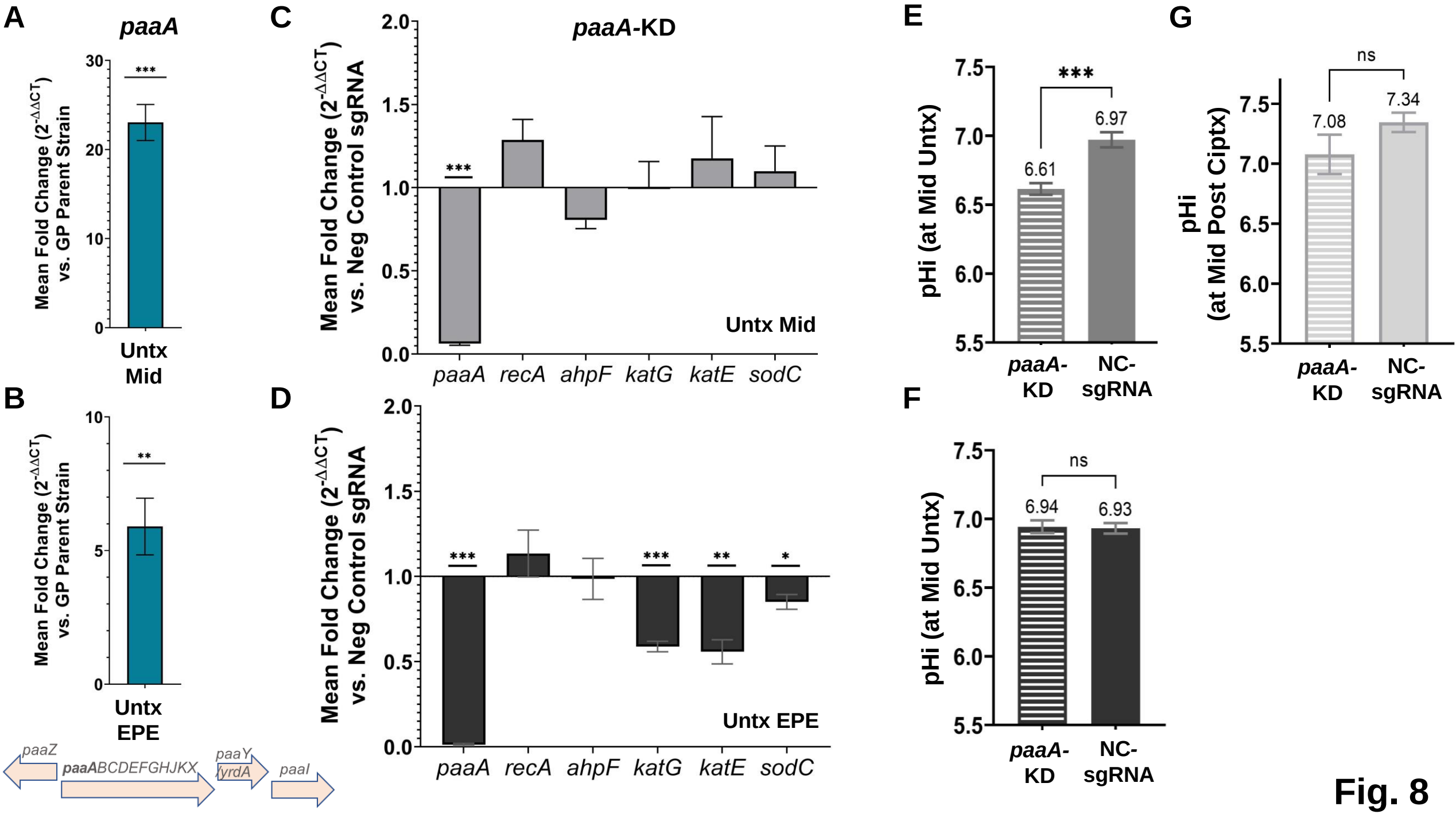
A
paaA
Mean Fold Change (2^-ΔΔCT) vs. GP Parent Strain
30
20
10
0
***
Untx Mid
B
10
5
0
**
Untx EPE
paaZ
paaABCDEFGHJKX
paaY
yrdA
paaI
C
paaA-KD
Mean Fold Change (2^-ΔΔCT) vs. Neg Control sgRNA
2.0
1.5
1.0
0.5
0.0
***
Untx Mid
paaA recA ahpF katG katE sodC
D
Mean Fold Change (2^-ΔΔCT) vs. Neg Control sgRNA
***
***
**
*
Untx EPE
paaA recA ahpF katG katE sodC
E
pHi (at Mid Untx)
7.5
7.0
6.5
6.0
5.5
***
6.61
6.97
paaA-KD
NC-sgRNA
F
pHi (at Mid Untx)
ns
6.94
6.93
paaA-KD
NC-sgRNA
G
pHi (at Mid Post Ciptx)
ns
7.08
7.34
paaA-KD
NC-sgRNA

Fig. 8

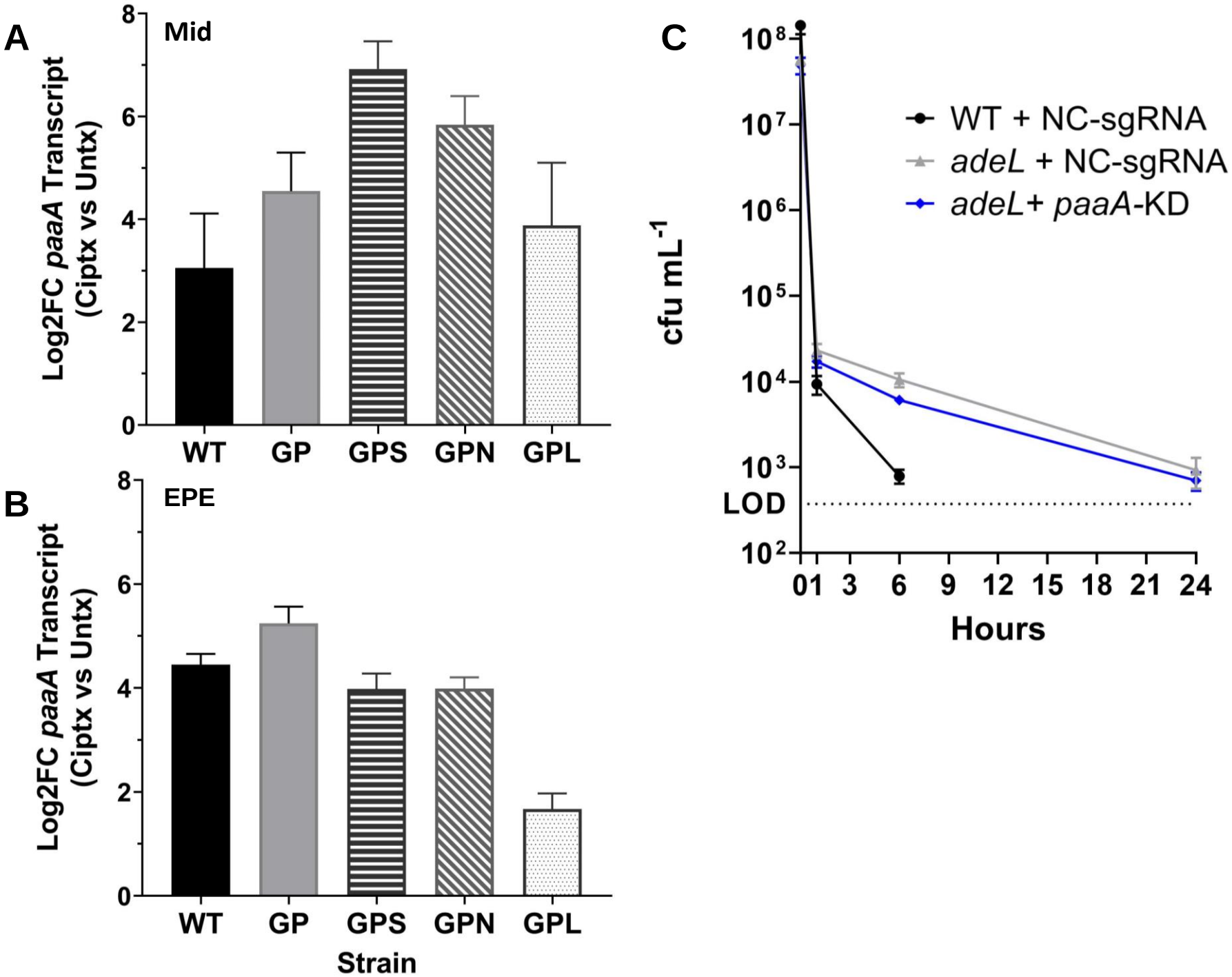
A
Mid
Log2FC paaA Transcript (Ciptx vs Untx)
0
2
4
6
8
WT
GP
GPS
GPN
GPL
B
EPE
Log2FC paaA Transcript (Ciptx vs Untx)
0
2
4
6
8
WT
GP
GPS
GPN
GPL
Strain
C
cfu mL-1
10^8
10^7
10^6
10^5
10^4
10^3
LOD
10^2
WT + NC-sgRNA
adeL + NC-sgRNA
adeL+ paaA-KD
0 1 3 6 9 12 15 18 21 24
Hours

Fig. 9

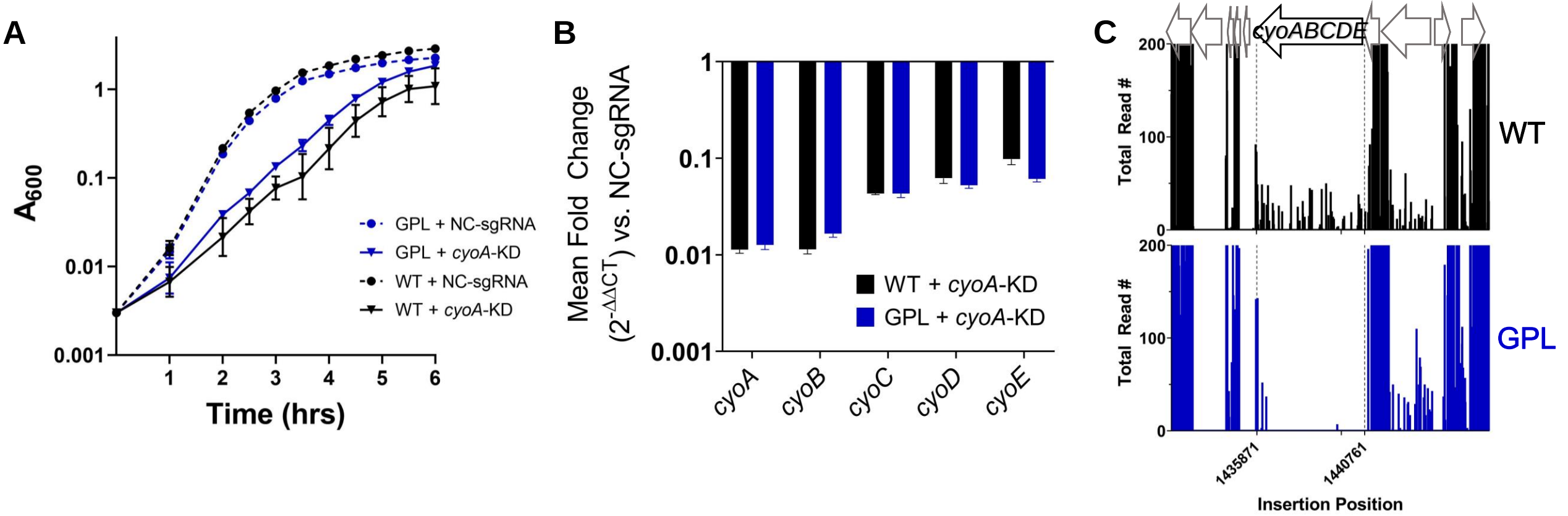
A
A_{600}
1
0.1
0.01
0.001
1
2
3
4
5
6
Time (hrs)
GPL + NC-sgRNA
GPL + cyoA-KD
WT + NC-sgRNA
WT + cyoA-KD
B
Mean Fold Change
($2^{-\Delta\Delta CT}$) vs. NC-sgRNA
1
0.1
0.01
0.001
WT + cyoA-KD
GPL + cyoA-KD
cyoA
cyoB
cyoC
cyoD
cyoE
C
cyoABCDE
Total Read #
200
100
0
WT
GPL
1435871
1440761
Insertion Position

Supp. Fig. 1

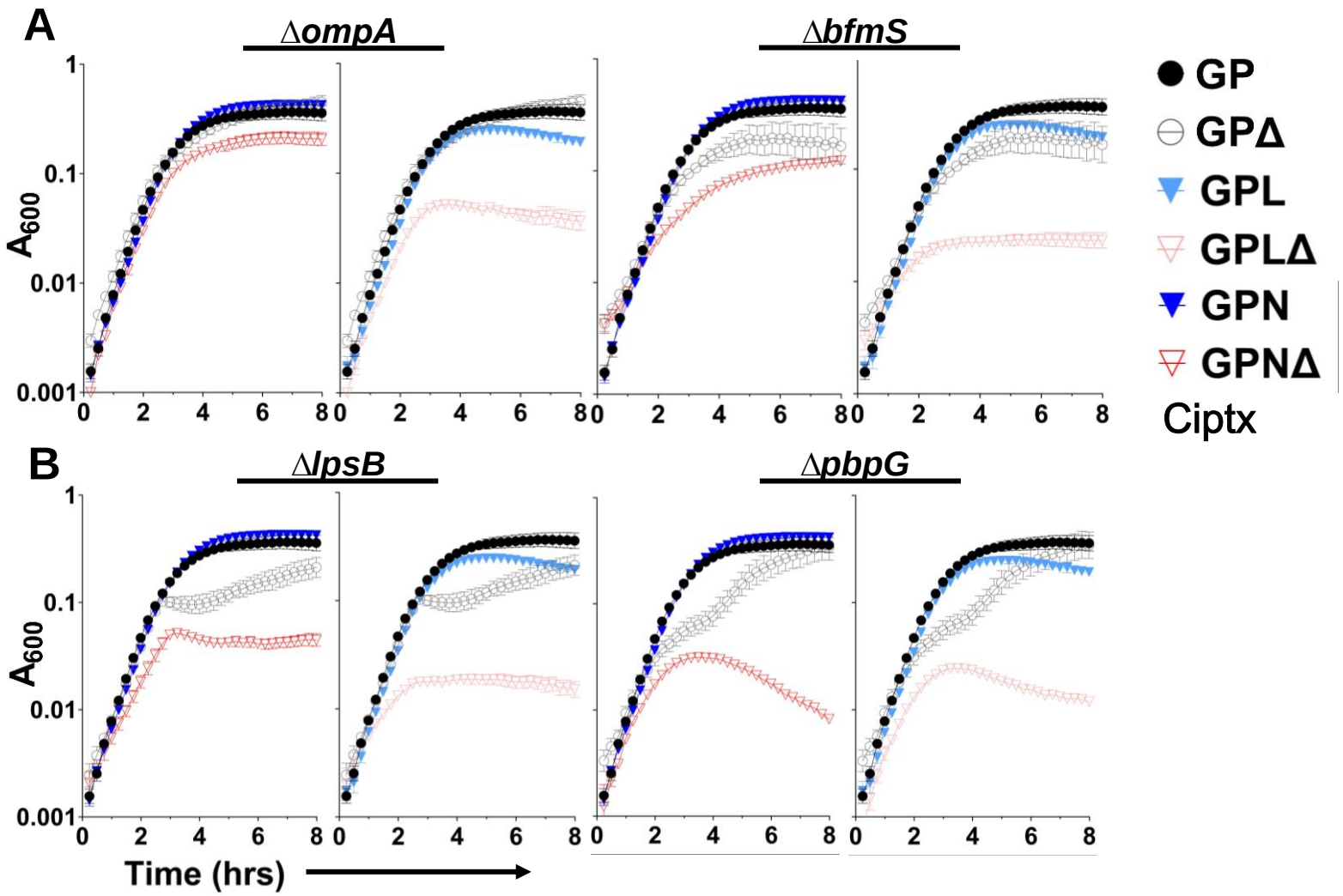
A
ΔompA
ΔbfmS
B
ΔlpsB
ΔpbpG
A600
1
0.1
0.01
0.001
0
2
4
6
8
Time (hrs)
GP
GPΔ
GPL
GPLΔ
GPN
GPNΔ
Ciptx

Supp. Fig. 2

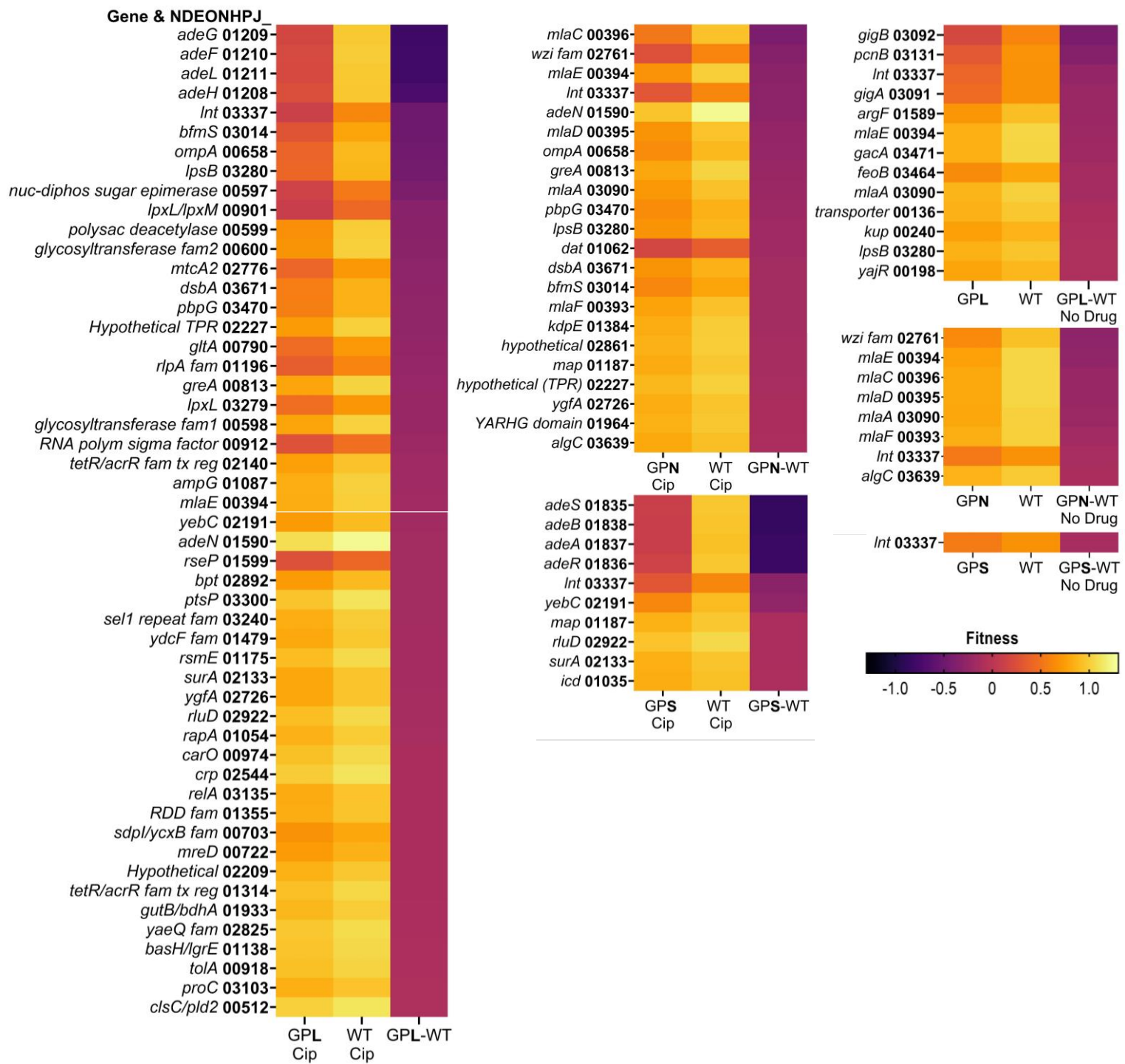
Gene & NDEONHPJ_
adeG 01209
adeF 01210
adeL 01211
adeH 01208
Int 03337
bfmS 03014
ompA 00658
lpsB 03280
nuc-diphos sugar epimerase 00597
lpxL/lpxM 00901
polysac deacetylase 00599
glycosyltransferase fam2 00600
mtcA2 02776
dsbA 03671
pbpG 03470
Hypothetical TPR 02227
gltA 00790
rlpA fam 01196
greA 00813
lpxL 03279
glycosyltransferase fam1 00598
RNA polym sigma factor 00912
tetR/acrR fam tx reg 02140
ampG 01087
mlaE 00394
yebC 02191
adeN 01590
rseP 01599
bpt 02892
ptsP 03300
sel1 repeat fam 03240
ydcF fam 01479
rsmE 01175
surA 02133
ygfA 02726
rluD 02922
rapA 01054
carO 00974
crp 02544
relA 03135
RDD fam 01355
sdpI/ycxB fam 00703
mreD 00722
Hypothetical 02209
tetR/acrR fam tx reg 01314
gutB/bdhA 01933
yaeQ fam 02825
basH/lgrE 01138
tolA 00918
proC 03103
clsC/pld2 00512
GPL Cip
WT Cip
GPL-WT
mlaC 00396
wzi fam 02761
mlaE 00394
Int 03337
adeN 01590
mlaD 00395
ompA 00658
greA 00813
mlaA 03090
pbpG 03470
lpsB 03280
dat 01062
dsbA 03671
bfmS 03014
mlaF 00393
kdpE 01384
hypothetical 02861
map 01187
hypothetical (TPR) 02227
ygfA 02726
YARHG domain 01964
algC 03639
GPN Cip
WT Cip
GPN-WT
adeS 01835
adeB 01838
adeA 01837
adeR 01836
Int 03337
yebC 02191
map 01187
rluD 02922
surA 02133
icd 01035
GPS Cip
WT Cip
GPS-WT
gigB 03092
pcnB 03131
Int 03337
gigA 03091
argF 01589
mlaE 00394
gacA 03471
feoB 03464
mlaA 03090
transporter 00136
kup 00240
lpsB 03280
yajR 00198
GPL
WT
GPL-WT No Drug
wzi fam 02761
mlaE 00394
mlaC 00396
mlaD 00395
mlaA 03090
mlaF 00393
Int 03337
algC 03639
GPN
WT
GPN-WT No Drug
Int 03337
GPS
WT
GPS-WT No Drug
Fitness
-1.0
-0.5
0
0.5
1.0

Supp. Fig. 3

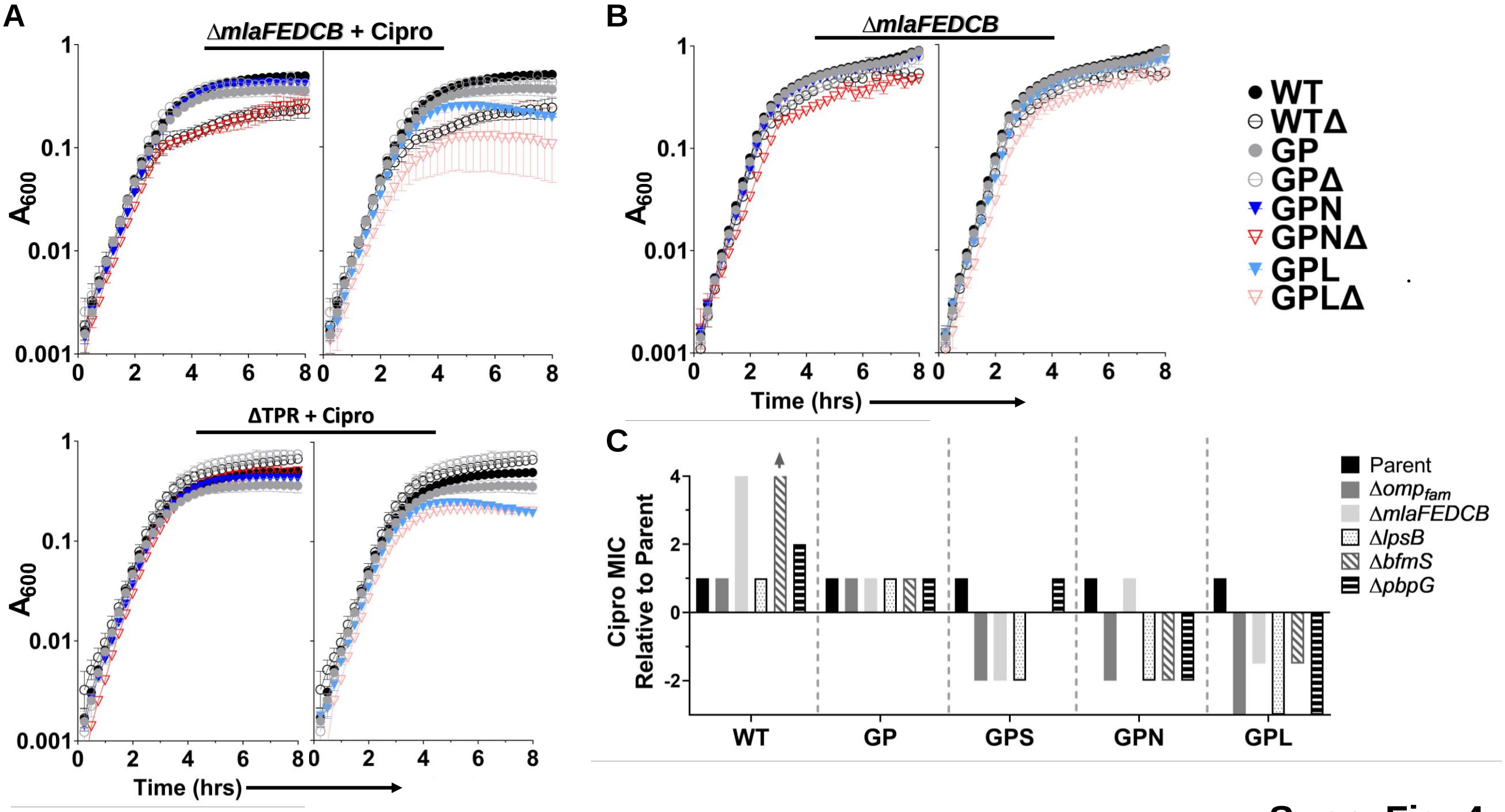
A
ΔmlaFEDCB + Cipro
ΔTPR + Cipro
A600
1
0.1
0.01
0.001
0
2
4
6
8
Time (hrs)
B
ΔmlaFEDCB
WT
WTΔ
GP
GPΔ
GPN
GPNΔ
GPL
GPLΔ
C
Cipro MIC
Relative to Parent
4
2
0
-2
WT
GP
GPS
GPN
GPL
Parent
Δomp_fam
ΔmlaFEDCB
ΔlpsB
ΔbfmS
ΔpbpG

Supp. Fig. 4

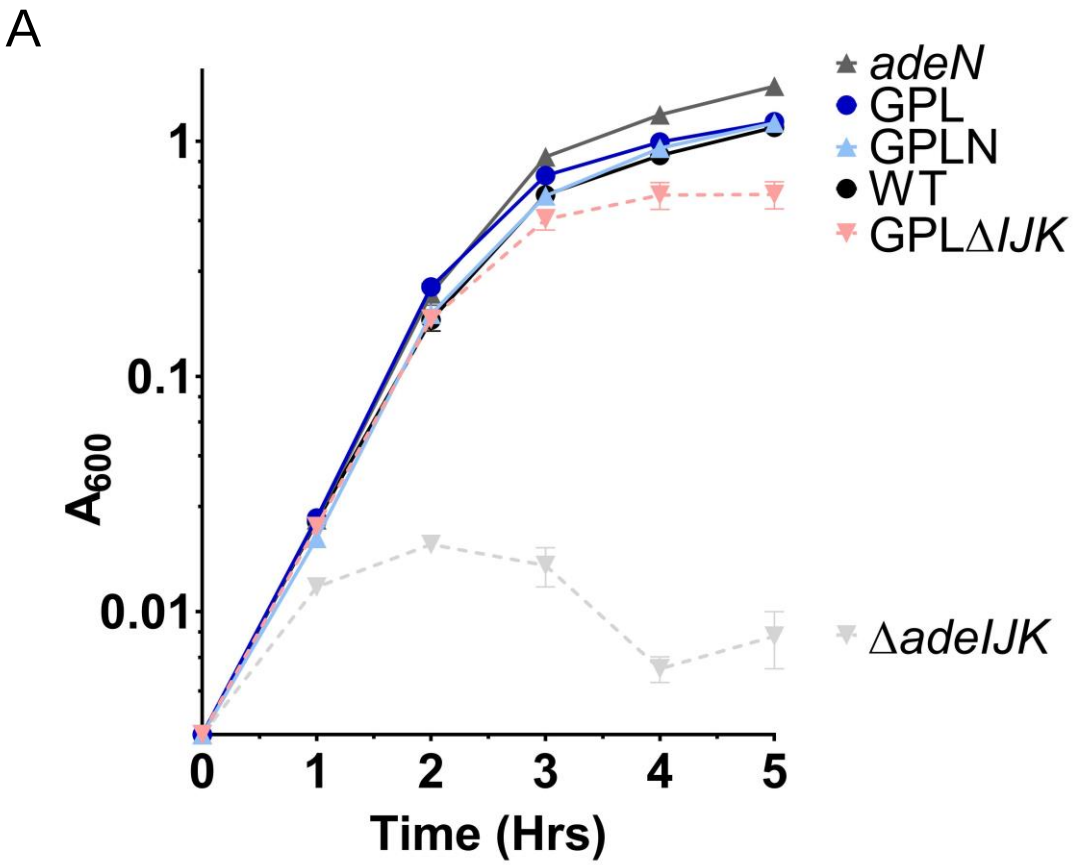
A
adeN
GPL
GPLN
WT
GPLΔIJK
ΔadeIJK
1
0.1
0.01
A600
0
1
2
3
4
5
Time (Hrs)

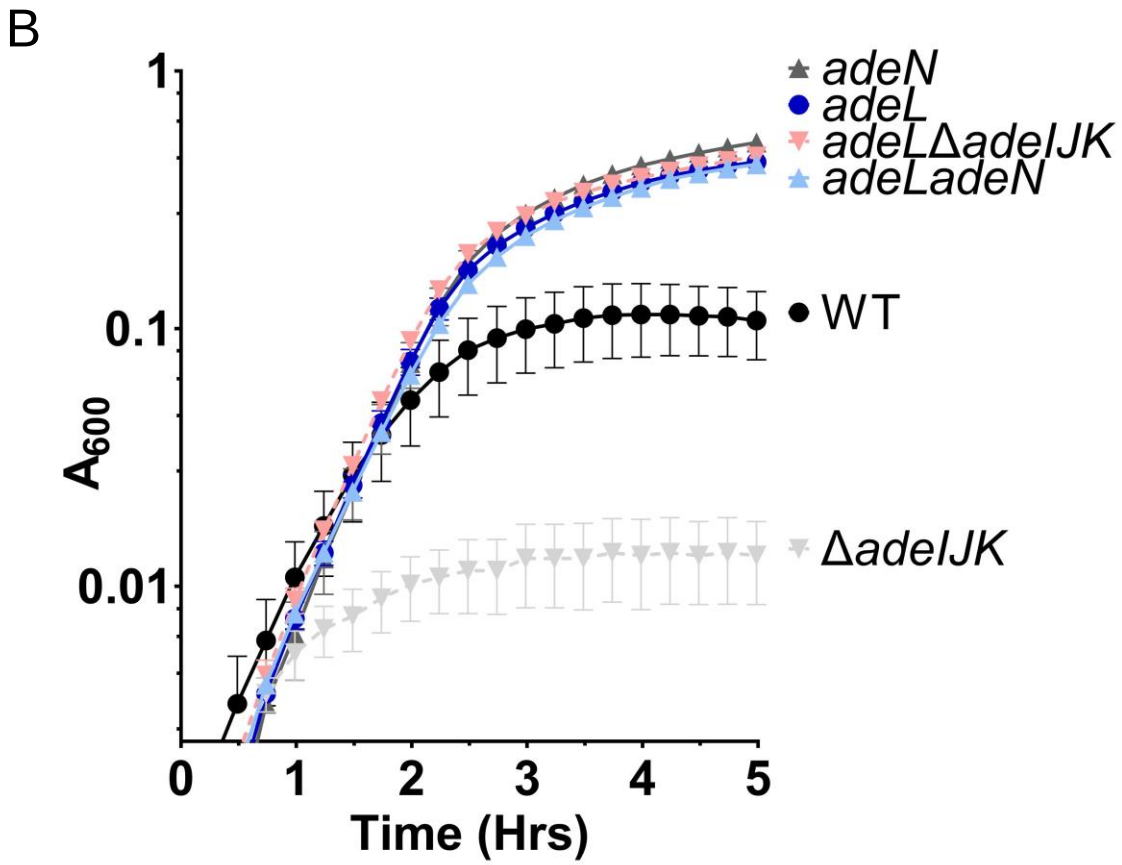
B
adeN
adeL
adeLΔadeIJK
adeLadeN
WT
ΔadeIJK
1
0.1
0.01
A600
0
1
2
3
4
5
Time (Hrs)

Supp. Fig. 5